Author Manuscript

Author Manuscript

Author Manuscript

Author Manuscript

HHS Public Access

Author manuscript

Nature. Author manuscript; available in PMC 2016 December 06.

Published in final edited form as:

Nature. ; 534(7608): 494–499. doi:10.1038/nature17976.

Selective spider toxins reveal a role for $Na_v1.1$ channel in mechanical pain

Jeremiah D. Osteen[1], **Volker Herzig**[2], **John Gilchrist**[3], **Joshua J. Emrick**[1], **Chuchu Zhang**[1], **Xidao Wang**[4], **Joel Castro**[5,6], **Sonia Garcia-Caraballo**[5,6], **Luke Grundy**[5,6], **Grigori Y. Rychkov**[6], **Andy D. Weyer**[7], **Zoltan Dekan**[2], **Eivind A. B. Undheim**[2], **Paul Alewood**[2], **Cheryl L. Stucky**[7], **Stuart M. Brierley**[5,6], **Allan I. Basbaum**[4], **Frank Bosmans**[3], **Glenn F. King**[2], and **David Julius**[1]

[1]Department of Physiology, University of California, San Francisco, CA 94143, USA

[2]Institute for Molecular Bioscience, University of Queensland, St Lucia, Queensland 4072, Australia

[3]Department of Physiology and Solomon H. Snyder Department of Neuroscience, Johns Hopkins University School of Medicine, Baltimore, MD 21205, USA

[4]Department of Anatomy, University of California, San Francisco, CA 94143, USA

[5]Visceral Pain Group, University of Adelaide, South Australian Health and Medical Research Institute (SAHMRI), North Terrace, Adelaide, SA 5000, Australia

[6]Centre for Nutrition and Gastrointestinal Diseases, Discipline of Medicine, University of Adelaide, South Australian Health and Medical Research Institute (SAHMRI), North Terrace, Adelaide, SA 5000, Australia

[7]Department of Cell Biology, Neurobiology, and Anatomy, Medical College of Wisconsin, Milwaukee, Wisconsin 53226

Abstract

Voltage-gated sodium (Na_v) channels initiate action potentials in most neurons, including primary afferent nerve fibers of the pain pathway. Local anesthetics block pain through non-specific

Users may view, print, copy, and download text and data-mine the content in such documents, for the purposes of academic research, subject always to the full Conditions of use: http://www.nature.com/authors/editorial_policies/license.html#terms

Correspondence and requests for materials should be addressed to D.J. (david.julius@ucsf.edu), G.K (glenn.king@imb.uq.edu.au), or F.B. (frankbosmans@jhmi.edu).

Author contributions

J.D.O., V.H., E.A.B.U., G.K. and D.J. carried out venom collection and screening, toxin purification and characterization. Z.D. and P.A. carried out Hm1a synthesis. J.D.O., J.G., C.Z., D.J. and F.B. designed, performed, and analyzed electrophysiological and calcium imaging experiments to determine toxin mechanism and selectivity. J.J.E., J.D.O., X.W. A.I.B, and D.J. designed, performed and analyzed histological experiments. A.D.W. and C.L.S. designed, performed, and analyzed skin-nerve recordings. X.W., J.D.O., D.J., and A.I.B. designed, performed, and analyzed behavioral experiments to assess somatic function. J.C., S.G-C., L.G., G.Y.R. and S.M.B. designed, performed and analyzed studies relating to colonic afferent and patch clamp pharmacological studies. All authors contributed to the discussion and interpretation of the results. J.D.O. and D.J. wrote the manuscript with contributions and suggestions from all authors.

Sequences and activity profiles for Hm1a and Hm1b can be found in the ArachnoServer database under accession numbers AS000224 and AS002363, respectively.

The authors declare competing financial interests: details are available in the online version of the paper.

Author Manuscript Author Manuscript Author Manuscript Author Manuscript

actions at all Na_v channels, but the discovery of selective modulators would facilitate the analysis of individual subtypes and their contributions to chemical, mechanical, or thermal pain. Here, we identify and characterize spider toxins that selectively activate the $Na_v1.1$ subtype, whose role in nociception and pain has not been explored. We exploit these probes to demonstrate that $Na_v1.1$-expressing fibers are modality-specific nociceptors: their activation elicits robust pain behaviors without neurogenic inflammation and produces profound hypersensitivity to mechanical, but not thermal, stimuli. In the gut, high-threshold mechanosensitive fibers also express $Na_v1.1$ and show enhanced toxin sensitivity in a model of irritable bowel syndrome. Altogether, these findings establish an unexpected role for $Na_v1.1$ in regulating the excitability of sensory nerve fibers that underlie mechanical pain.

Pain is a multimodal system in which activation of functionally distinct sensory nerve fibers elicits acute, protective reflexes, as well as maladaptive responses that contribute to persistent pain[1]. In these nociceptive neurons, three voltage-gated sodium (Na_v) channels – $Na_v1.7$, $Na_v1.8$ and $Na_v1.9$ – have garnered particular attention because mutations affecting these subtypes are associated with insensitivity to pain or persistent pain syndromes[2–6]. $Na_v1.1$ is also expressed by somatosensory neurons[7–10], but no link has been established between this subtype and nociception[11]. Mutations affecting $Na_v1.1$ are associated with central nervous system (CNS) disorders such as epilepsy[12,13], autism[14], and Alzheimer's[15], and these clinically dominant phenotypes may have masked roles for this subtype in peripheral neurons. For example, gain-of-function mutations in $Na_v1.1$ underlie familial hemiplegic migraine type 3 (ref. 16), and while this phenotype has been ascribed to a CNS-initiated mechanism[17], dysfunction in sensory neurons may also contribute to this pain syndrome.

Another challenge to parsing out roles for $Na_v1.1$ in pain is that of developing subtype-selective drugs for any member of this highly conserved family of ion channels[18]. Natural products can be exploited as a source of evolutionarily honed agents that target receptors with exquisite specificity. Such agents may be found in complex venoms from spiders, scorpions, cone snails, and snakes, including toxins that excite sensory nociceptors to elicit pain or discomfort in offending predators[19,20]. Here we describe two algogenic tarantula toxins that selectively activate $Na_v1.1$ to elicit acute pain and mechanical allodynia, providing new insights into specific roles for this channel and $Na_v1.1$-expressing sensory nerve fibers in nociception and pain hypersensitivity.

Selective $Na_v1.1$ activating toxins

To identify novel toxins that target nociceptors, we used calcium imaging to screen through >100 spider, scorpion and centipede venoms for the ability to activate cultured somatosensory neurons. Venom from the tarantula *Heteroscodra maculata* (Fig. 1a) robustly excited a subset of neurons from trigeminal (TG) or dorsal root ganglia (DRG) from mice or rats. Venom fractionation yielded two active peptides, which were identified by MALDI-MS and Edman sequencing as inhibitor cysteine knot (ICK) peptides of related sequence (Extended Data Fig. 1a). We named these toxins δ-theraphotoxin-Hm1a (Hm1a) and δ-theraphotoxin-Hm1b (Hm1b). Application of synthetic Hm1a to rat DRG neurons likewise

Author Manuscript Author Manuscript Author Manuscript Author Manuscript

triggered calcium responses (Fig. 1b), validating Hm1a as an active venom component. All subsequent experiments were performed with synthetic Hm1a peptide unless otherwise stated.

Tetrodotoxin (TTX) blocked Hm1a-evoked calcium responses (Fig. 1b), suggesting involvement of Na_v channels. Indeed, whole-cell patch-clamp recordings from TG neurons showed that Hm1a robustly inhibited Na_v current inactivation (Fig. 1c). Among Na_v subtypes expressed by these neurons, only $Na_v1.1$, 1.6 and 1.7 are sensitive to TTX[21], narrowing our search. We next tested ICA-121431, a small molecule inhibitor with selectivity for $Na_v1.1$ and 1.3 subtypes[22] (Extended Data Fig. 1b), and found that it greatly diminished Hm1a-evoked calcium responses in both embryonic DRG and P0 mouse TG cultures (Fig. 1d and Extended Data Fig. 1c–d), suggesting that $Na_v1.1$ is the main target of Hm1a in somatosensory neurons. In contrast, ICA-121431 only partially blocked responses to SGTx1, an Hm1a-related peptide that shows little selectivity among Na_v subtypes[23] and excites a larger cohort of sensory neurons compared to Hm1a (Extended Data Fig. 1c–d). To confirm toxin selectivity for $Na_v1.1$, we heterologously expressed $Na_v1.1$–1.8 α subunits in *Xenopus* oocytes. Indeed, Hm1a potently inhibited $hNa_v1.1$ inactivation (EC_{50} = 38 ± 6 nM), with substantially weaker effects on $hNa_v1.2$ and $hNa_v1.3$, and no effect on $hNa_v1.4$–1.8 (Fig. 1e and Extended Data Fig. 1e). Similar results were obtained with native Hm1b (Extended Data Fig. 1f). $Na_v1.9$ is not efficiently expressed in recombinant systems, but surrogate chimeras ($rK_v2.1$ channels containing the S3b-S4 toxin-binding region from each of the four $hNa_v1.9$ domains) were also toxin insensitive (Extended Data Fig. 1g)[24].

Hm1b is a novel toxin, but Hm1a was previously described as κ-theraphotoxin-Hm1a, a moderate-affinity blocker of $K_v4.1$ voltage-gated potassium (K_v) channels[25]. We found, however, that high concentrations (up to 5 μM) of synthetic Hm1a blocked ≤20% of $mK_v4.1$ current (Extended Data Fig. 1h), and 1 μM native Hm1a displayed a saturating effect on $Na_v1.1$, but failed to block $mK_v4.1$ (Extended Data Fig. 1h). Moreover, in cultured sensory neurons, outward K^+ currents were unaffected by 500 nM Hm1a, suggesting that its main physiologic target is $Na_v1.1$. This may explain why injection of Hm1a into the mouse brain elicits convulsions and rapid death[25]. Taken together, these results demonstrate that Hm1a activates a subset of sensory neurons by selectively targeting $Na_v1.1$.

Analysis of Hm1a-responsive TG neurons in whole-cell current clamp configuration showed toxin-evoked hyperexcitability (Fig. 1f). Hm1a did not alter resting membrane potential (before Hm1a, Vm = −55 ± 6 mV; after Hm1a, Vm = −56 ± 6 mV), however, it robustly enhanced spike frequency during a 20 pA current injection. Hm1a also significantly prolonged the action potential width (by 28.3 ± 8.4%; from 6.5 to 8.6 msec), consistent with introduction of non-inactivating sodium current (Fig. 1f). We found that toxin responses were most robust in sensory neuron cultures derived from young (embryonic or newborn) mice or rats, likely reflecting a lower threshold for action potential firing in these cells or culture conditions. Indeed, we found that prostaglandin E2 (PGE2) sensitization[26] of adult neurons prior to toxin exposure greatly enhanced the percentage of toxin sensitive cells (Extended Data Fig. 1i), consistent with this hypothesis.

Author Manuscript Author Manuscript Author Manuscript Author Manuscript

Selectivity depends on DIV S1-S2 loop

Our data suggest that Hm1a inhibits both the speed and extent of fast inactivation (Fig. 2a), similar to the mechanism described for less selective peptide toxins that bind to the S3b-S4 voltage sensor region of domain IV (DIV)[23]. To determine whether Hm1a targets the same locale, we transferred each of four S3b-S4 regions from $hNa_v1.1$ into the cognate location of the homo-tetrameric $rK_v2.1$ voltage-gated potassium channel, which is normally insensitive to the toxin (Extended Data Fig. 2a). Indeed, transfer of just the DIV S3b-S4 region rendered $rK_v2.1$ sensitive to Hm1a, demonstrating that this segment is a primary determinant of toxin action (Fig. 2b and Extended Data Fig. 2b). However, this region is identical or highly conserved in $hNa_v1.1$, 1.2 and 1.3, and thus cannot fully account for toxin selectivity. To identify other functionally important regions, we constructed chimeras between $Na_v1.1$ and $Na_v1.4$, the latter being completely insensitive to Hm1a. Replacement of the S3b-S4 region of $hNa_v1.4$ with that from $hNa_v1.1$ did not confer toxin sensitivity, whereas transfer of both S3b-S4 and the S1-S2 loop resulted in full toxin sensitivity (Fig. 2c and Extended Data Fig. 2c–e). These results indicate that both domains together determine toxin sensitivity and subtype selectivity, consistent with previous suggestions that S1-S2 contributes to toxin recognition sites on voltage sensors[27,28].

$Na_v1.1$ is found on myelinated Aδ fibers

Using *in situ* hybridization histochemistry, we found that $Na_v1.1$ transcripts are expressed primarily by medium-diameter sensory neurons constituting 35% of all cells, most of which (>75%) belong to the myelinated (NF200-positive) cohort (Fig. 3). In contrast, we observed limited (5–11%) overlap of $Na_v1.1$-positive cells with markers of small diameter, unmyelinated neurons, including TRPV1, CGRP, tyrosine hydroxylase, and the lectin IB4. However, we did see substantial co-expression with the 5-HT_3 receptor (43% of $Na_v1.1$-positive cells express 5-HT_3), a marker of lightly myelinated Aδ neurons[29]. Finally, 22% of $Na_v1.1$-positive cells also expressed the cold/menthol receptor, TRPM8, which is found in both C and Aδ fibers[30]. Taken together, we conclude that $Na_v1.1$ is expressed primarily by myelinated neurons, including Aδ fibers, consistent with previous histological and transcriptome profiling data [7,31]. We also characterized Hm1a-sensitive neurons for responses to other receptor-selective agonists (Extended Data Fig. 3b), further confirming this assignment. Interestingly, most (>85%) $Na_v1.1$-positive cells also expressed $Na_v1.7$, suggesting that this population of myelinated neurons contributes to nociception (see below).

We next explored the effect of Hm1a on mechanonociceptive Aδ fibers (AMs) using the *ex vivo* skin-nerve preparation. We found that application of 1μM Hm1a to cutaneous receptive fields significantly increased firing rate in these AM fibers in response to mechanical stimuli (Fig. 3d), confirming expression of functional $Na_v1.1$ in this afferent population. Previous studies found limited expression of TRPV1 in AM fibers[33], consistent with our findings of limited overlap between $Na_v1.1$ and TRPV1. Taken together, these functional data confirm our histological assignment of $Na_v1.1$ expression to myelinated Aδ fibers, and further suggest that $Na_v1.1$ participates in mechanical nociception.

Author Manuscript Author Manuscript Author Manuscript Author Manuscript

Hm1a elicits pain and touch sensitivity

Does activation of $Na_v1.1$-expressing fibers produces pain behaviors? Indeed, injection of Hm1a (5μM in 10μl) into the mouse hind paw elicited immediate and robust nocifensive responses (bouts of licking or biting of the injected paw) throughout the observation period (Fig. 4a). Toxin injection also significantly increased Fos immunoreactivity in dorsal horn neurons of the superficial lamina ipsilateral to the injection, signifying functional engagement of nociceptors and their central connections (Fig. 4b). To exclude the possibility that this depends on the small population of fibers co-expressing TRPV1 and $Na_v1.1$, we ablated TRPV1-positive terminals by intrathecal (spinal) injection of capsaicin[34], in which case Hm1a-evoked nocifensive behavior persisted (Fig. 4a). Remarkably, Hm1a did not produce swelling or plasma extravasation of the injected paw, a neurogenic inflammatory response readily provoked by activation of peptidergic C-fiber nociceptors that include most TRPV1-expressing neurons (Fig. 4c). These results further suggest that Hm1a elicits pain by activating a non-peptidergic subset of myelinated sensory fibers.

Genetic or pharmacologic elimination of TRPV1-expressing fibers greatly diminishes sensitivity to noxious heat, but does not perturb sensitivity to mechanical stimuli[34–36]. In light of the anatomical and physiological results described above, we asked whether Hm1a has differential effects on these modalities by monitoring responses to thermal and mechanical stimuli following intraplantar injection of toxin at a dose (500nM in 10μl) insufficient to elicit acute behavior. Indeed, intraplantar injection of Hm1a did not alter sensitivity to heat, but produced robust sensitization to mechanical stimulation that was not dependent on TRPV1-expressing fibers (Fig. 4d, e). Equivalent mechanical sensitization was also observed following injection of native Hm1b peptide (Fig. 4e). In agreement with these behavioral observations, we found that all Hm1a-responsive adult DRG neurons displayed mechanically activated currents, except for those neurons that were also capsaicin sensitive (Fig. 4f).

To confirm the requirement of $Na_v1.1$ in toxin-evoked behaviors, we crossed mice bearing a floxed $Na_v1.1$ allele[13] to a line expressing Cre recombinase under control of the peripherin promoter, which is active in a large percentage of unmyelinated and myelinated sensory neurons during development[37]. Indeed, analysis of a peripherin-Cre x YFP reporter line showed that these animals express Cre recombinase in 46% of $Na_v1.1$-positive cells (Extended Data Fig. 4a, b). Strikingly, elimination of $Na_v1.1$ from this subset of fibers significantly attenuated toxin-evoked behaviors, including both acute nocifensive responses and mechanical sensitization (Fig. 4a, e).

Robust activation of nociceptive pathways by nerve injury or inflammation can trigger both primary and secondary sensitization, the latter of which can manifest as mechanical or heat hypersensitivity contralateral to the insult[38,39]. In fact, we found that unilateral injection of Hm1a produced robust and equivalent mechanical sensitization of both the injected and contralateral paw (Fig. 4e). This contralateral sensitization was also modality specific as no change in heat sensitivity was observed (Fig. 4d). Importantly, Hm1a-mediated mechanical sensitivity was equivalently reduced in ipsilateral and contralateral paws of $Na_v1.1$-peripherin Cre animals, demonstrating that contralateral effects depend on $Na_v1.1$ (Fig. 4e).

Author Manuscript Author Manuscript Author Manuscript Author Manuscript

Since we did not observe signs of neurogenic inflammation, we asked whether this phenotype results from Hm1a-mediated nerve injury. However, this seems unlikely since toxin injection failed to induce expression of ATF3, a marker of nerve damage[40] (Extended Data Fig. 4c). Taken together, these observations demonstrate that direct activation of $Na_v1.1$-expressing fibers is sufficient to produce robust and modality-specific bilateral sensitization.

$Na_v1.1$ and irritable bowel syndrome

Chronic mechanical hypersensitivity underlies the development of abdominal pain in patients with irritable bowel syndrome (IBS)[41]. Given the apparent role of $Na_v1.1$ in mechano-nociception, we asked if this channel is expressed by mechanically sensitive fibers of the gut, and if so, whether it contributes to neuronal sensitization in a model of chronic visceral mechanical hypersensitivity (CVH)[42]. We therefore examined mechanical responses in an *ex vivo* gut-nerve preparation from healthy or CVH mice. In preparations from healthy animals, Hm1a increased mechanically-evoked spiking in a sub-population (40%) of high-threshold colonic afferents that constitute presumptive mechano-nociceptors (Fig. 5a and Extended Data Fig. 5a). Correspondingly, ICA-121431 reduced mechanical responses in 50% of fibers examined and blocked Hm1a sensitization (Fig. 5a and Extended Data Fig. 5a). Moreover, Hm1a significantly reduced the threshold for action potential firing in a subset (45%) of retrogradely traced colonic DRG neurons as measured by whole-cell current clamp analysis (Fig. 5b and Extended Data Fig. 5b). These results demonstrate that a subset of high-threshold mechanosensitive colonic fibers express functional $Na_v1.1$ channels.

In colonic afferents from CVH mice, baseline mechanosensory responses were elevated compared to healthy controls (compare Figs. 5a and 5c). Application of Hm1a enhanced mechanically-evoked spiking in a subset (36%) of CVH fibers beyond this already elevated level (Fig. 5c). Interestingly, in the context of CVH (and in contrast to normal controls), toxin application dramatically increased the electrical excitability of most (64%) retrogradely traced colonic DRG neurons (Fig. 5d), suggesting functional upregulation of $Na_v1.1$. Furthermore, ICA-121431 reduced mechanosensory responses in most (70%) CVH sensitized fibers to levels resembling those of baseline controls (compare Figs. 5a and 5c), and blocked the sensitizing effects of Hm1a (Fig. 5c). Taken together, these results support a role for $Na_v1.1$ in mechanical hypersensitivity in IBS.

Concluding remarks

Development of Na_v channel subtype-selective ligands is an important, but challenging goal. Our results identify a site within the DIV S1-S2 loop that enhances subtype selectivity, providing a potential strategy for designing other subtype-specific gating modifiers. Moreover, toxins such as Hm1a/b that alter inactivation may be of particular utility in boosting Na_v channel activity where partial loss-of-function has been linked to developmental or neurodegenerative disorders, such as autism, Alzheimer's or Dravet syndrome[14,15,43]. Analysis of toxin-channel interactions, including the multi-site nature of this pharmacophore, may shed new light on strategies for developing a broader class of molecules having a similar selectivity and functional profile.

Author Manuscript Author Manuscript Author Manuscript Author Manuscript

The critical role of $Na_v1.1$ in the brain may have prevented its prior recognition as a contributor to peripheral pain signaling. Our results now unambiguously implicate $Na_v1.1$ and $Na_v1.1$-expressing myelinated afferents in nociception. Activation or sensitization of these fibers is sufficient to elicit robust acute pain, as well as mechanical allodynia, without triggering neurogenic inflammation, distinguishing these fibers from well-characterized C-nociceptors. Previous studies have implicated myelinated Aδ fibers in mechano-nociception[44,45], and $Na_v1.1$ now provides an important new marker with which to more precisely identify the contribution of these fibers to acute and chronic pain.

Our findings with the CVH model suggest that pharmacological blockade of $Na_v1.1$ represents a novel therapeutic strategy for diminishing chronic pain associated with IBS, and perhaps other pain conditions associated with mechanical sensitization, including migraine headache. While $Na_v1.1$ activity in the brain may underlie aura in FHM3 patients[17], our results suggest that these gain-of-function mutations may also produce migraine pain through actions of $Na_v1.1$ in mechanical nociceptors. In fact, anticonvulsants that target Na_v channels, including $Na_v1.1$, have demonstrated efficacy in reducing migraine attacks in some individuals[46,47]. Moreover, rufinamide, an anticonvulsant that was recently shown to inhibit $Na_v1.1$ (ref. 48), has also been reported to diminish nerve-injury evoked mechanical allodynia[49]. Our findings therefore provide a mechanistic rationale for these actions, and motivate further analysis of $Na_v1.1$ and $Na_v1.1$-expressing nociceptors in acute and persistent pain.

Methods

Venom collection and screening

Venoms from spiders, scorpions and centipedes were collected by mild electrical stimulation of the chelicerae, telson or forcipules, respectively. Venoms were then lyophilized and kept frozen until use. Approximately 100 venoms were tested by ratiometric calcium imaging using a standard inverted microscope setup. Responses to high extracellular potassium (150mM), capsaicin (1 μM), or previously characterized venoms or purified toxins[19] were used to validate the health and robustness of sensory neuron cultures used in screening assays. Responses were digitized and analyzed using MetaMorph software (Molecular Devices). Venom-evoked responses that were stimulus-locked, visually detectable above background, and restricted to neurons (i.e. did not cause calcium entry into glia or fibroblasts) were selected for further analysis. Pharmacological analysis was used to narrow down potential targets and crude venoms or purified fractions were subsequently tested on cloned candidate channels. Candidates were taken forward based on the robustness of the response and evidence for selectivity at novel targets. See Supplementary Information for a summary of venoms that produced no detectible or specific response in our hands.

Hm1a/b isolation

Venom from *H. maculata* (1 mg dried) was fractionated on a C_{18} reversed-phase (RP) high-performance liquid chromatography (HPLC) column (Jupiter 250 × 4.6 mm, 5 mm; Phenomenex, Torrance, CA) on a Shimadzu (Shimadzu, Rydalmere, NSW, Australia) Prominence HPLC system. The following linear gradient of solvent B (90% acetonitrile

Author Manuscript Author Manuscript Author Manuscript Author Manuscript

(MeCN), 0.1% formic acid in water) in solvent A (0.1% formic acid in water) was used at a flow rate of 1 ml/min: 5% B for 5 min, then 5–20% B for 5 min followed by 20–40% B over 40 min. Absorbance was measured at 214 nm and 280 nm and collected fractions were lyophilized before storage at −20°C.

Mass Spectrometry

Peptide masses were determined by matrix-assisted laser desorption/ionization (MALDI) time of flight (TOF) mass spectrometry (MS) using a 4700 Proteomics Bioanalyzer model (Applied Biosystems, Carlsbad, CA). Peptides were dissolved in water and mixed 1:1 (v/v) with α-cyano-4-hydroxycinnamic acid matrix (7 mg/ml in 50% MeCN, 5% formic acid) and mass spectra acquired in positive reflector mode. All reported masses are for the monoisotopic $M+H^+$ ions.

Sequence determination

N-terminal sequencing was performed by the Australian Proteome Analysis Facility (Sydney, NSW, Australia). In brief, Hm1a (600 pmol) and Hm1b (250 pmol) were reconstituted and reduced by addition DTT (25 mM) followed by incubation at 56°C for 0.5 h. The samples were then alkylated using iodoacetamide (55 mM) at room temperature for 0.5 h and purified by RP-HPLC using a Zorbax 300SB-C18 column (3 × 150 mm). The target peaks of interest were identified, collected then reduced to minimal volume under vacuum. The entire sample was loaded onto a precycled, Biobrene-treated disc and subjected to 37 (Hm1a) or 42 (Hm1b) cycles of Edman N-terminal sequencing, respectively. Automated Edman degradation was carried out using an Applied Biosystems 494 Procise Protein Sequencing System.

Edman degradation of Hm1a yielded ECRYLFGGCSSTSDCCKHLSCRSDWKYCAWDGTF as the sequence, which has a calculated monoisotopic mass (for the $M+H^+$ ion) of 3908.58 Da. This is 86.97 Da short of the monoisotopic mass of Hm1a of 3995.55 Da. Hence, we conclude that a serine residue (87 Da) is missing on the C-terminal end of Hm1a to give a complete sequence of ECRYLFGGCSSTSDCCKHLSCRSDWKYCAWDGTFS. The complete sequence has a calculated monoisotopic mass (for the $M+H^+$ ion) of 3995.61 Da, which is only 0.06 Da different to the mass that was measured for the native Hm1a.

Edman degradation of Hm1b yielded ECRYLFGGCKTTADCCKHLGCRTDLYYCAWDGT as the sequence, which has a calculated monoisotopic mass (for the $M+H^+$ ion) of 3745.6 Da. This is 147 Da short of the monoisotopic mass of Hm1a of 3892.60 Da. We therefore conclude that an amidated phenylalanine is missing on the C-terminal end of Hm1b to give a complete sequence of ECRYLFGGCKTTADCCKHLGCRTDLYYCAWDGTF-NH_2. To confirm that the C-terminus of Hm1b is amidated, we digested native Hm1b with carboxypeptidase Y (CPY) and monitored the reaction by MALDI-TOF to identify the mass of the C-terminal residue as described previously[51]. 5 μL of 800 ng/μL native Hm1b in 100 mM ammonium acetate, pH 5.5, was incubated with 2 ng/μL CPY at 37 °C for 20 min. The reaction was monitored by removing 0.4 μL at 0, 1, 5, 10 and 20 min and spotting it on a MALDI plate with equal

Author Manuscript Author Manuscript Author Manuscript Author Manuscript

volume of 7 mg/mL α-cyano-4-hydroxycinnamic acid in 60% (*v/v*) acetonitrile, 5% formic acid (FA). Dried spots were washed with 10 μL 1% FA and allowed to dry before they were analyzed by MALDI-TOF-MS on a 4700 Proteomics Bioanalyser (Applied Biosciences, Foster City, CA, USA), acquiring spectra in reflector positive mode. The first CPY-mediated cleavage yielded a mass difference of 146 Da, which corresponds to an amidated phenylanine residue. Thus, the complete sequence has a calculated monoisotopic mass (for the $M+H^+$ ion) of 3892.64 Da, matching the native Hm1b.

Hm1a synthesis

Solvents for reversed-phase HPLC consisted of 0.05% TFA/H_2O (solvent A) and 90% MeCN/0.043% trifluoroacetic acid (TFA)/H_2O (solvent B). Analytical HPLC was performed on a Shimadzu LC20AT system using a Thermo Hypersil GOLD 2.1 × 100 mm C18 column heated at 40°C with flow rate of 0.3 mL/min. A gradient of 10 to 55% B over 30 min was used, with detection at 214 nm. Preparative HPLC was performed on a Vydac 218TP1022 column running at a flow rate of 16 mL/min using a gradient of 10 to 50% solvent B over 40 min. Mass spectrometry was performed on an API2000 (ABI Sciex) mass spectrometer in positive ion mode. All reagents were obtained commercially and were used without further purification.

Hm1a was synthesized using regioselective disulfide-bond formation[52–54]. The peptide was assembled on a 0.1 mmol scale using a Symphony (Protein Technologies Inc.) automated peptide synthesiser and a H-Ser(tBu)-2-ClTrt (loading 0.69 mmol/g) polystyrene resin. Couplings were performed in dimethylformamide (DMF) using 5 equivalents of Fmoc-amino acid/(2-(1H-benzotriazol-1-yl)-1,1,3,3-tetramethyluronium hexafluorophosphate (HBTU)/*N,N*-diisopropylethylamine (DIEA) (1:1:1) relative to resin loading for 2 × 20 min. Fmoc deprotection was achieved using 30% piperidine/DMF (1 × 1.5 min, then 1 × 4 min). Non-cysteine amino acid side-chains were protected as Asp(OtBu), Arg(Pbf), Glu(OtBu), His(Trt), Lys(Boc), Ser(tBu), Thr(tBu), Trp(Boc) and Tyr(tBu). The cysteine side chains were protected as Cys2,Cys16(Meb), Cys9,Cys21(Dpm), and Cys15,Cys28(Trt). Cleavage from the resin was achieved by treatment with 10% acetic acid (AcOH)/10% trifluoroethanol (TFE)/dichloromethane (DCM) at room temperature for 1 h. The product was precipitated and washed with *n*-hexane then lyophilized from 1,4-dioxane/MeCN/H_2O.

The first disulfide bond (Cys15–Cys28) was formed by dissolving the crude product in in HFIP (5 mL) and adding dropwise to a stirred solution of I_2 (4 equiv) in 10% 1,1,1,3,3,3-hexafluoropropan-2-ol (HFIP)/DCM (20 mL) over 5 min. Stirring was continued for a further 5 min then the solution was poured into a solution of ascorbic acid/sodium acetate in H_2O. The aqueous phase was extracted with DCM, and the combined organic layers washed with water. Following removal of solvent under reduced pressure, the product was lyophilized from 1,4-dioxane/MeCN/H_2O. ESI-MS (*m/z*): calc. (avg) 2159.4 $[M+3H]^{3+}$, found 2159.7.

The remaining side chain protecting groups [except Cys(Meb)] were removed by treatment with 95% TFA/2.5% triisopropylsilane (TIPS)/2.5% H_2O at room temperature for 2 h. After most of the cleavage solution was evaporated under a stream of N_2, the product was precipitated and washed with cold Et_2O and lyophilized from 50% MeCN/0.1% TFA/H_2O to

Author Manuscript Author Manuscript Author Manuscript Author Manuscript

give Cys2,Cys16(Meb), Cys9,Cys21(SH), Cys15–Cys28(SS) Hm1a (280 mg). ESI-MS (*m/z*): calc. (avg) 1404.3 $[M+3H]^{3+}$, found 1404.1.

The second disulfide bond (Cys9–Cys21) was formed by dissolving the crude product from the previous step in 30% DMSO/0.1 M HCl (0.5 mg/mL) and stirring at room temperature for 24 h. Cys2,16(Meb), Cys9–Cys21(SS), Cys15–Cys28(SS) Hm1a was then isolated by preparative HPLC (30 mg). ESI-MS (*m/z*): calc. (avg) 1403.6 $[M+3H]^{3+}$, found 1403.3.

Formation of the third disulfide bond (Cys2–Cys16) was then achieved by first removing the Cys(Meb) groups by treatment with HF/*p*-cresol (9:1) at 0°C for 1 h. The product was precipitated and washed with cold Et_2O and lyophilized from 50% MeCN/0.1% TFA/H_2O yielding Cys2,16(SH), Cys9–Cys21(SS), Cys15–Cys28(SS) Hm1a (24 mg). ESI-MS (*m/z*): calc. (avg) 1334.1 $[M+3H]^{3+}$, found 1333.7. Oxidation of the liberated thiols was performed using 30% DMSO/0.1 M HCl as described for the second disulfide bond to yield fully oxidised Hm1a (3 mg) that was indistinguishable by analytical HPLC from an authentic sample. ESI-MS (*m/z*): calc. (avg) 1333.5 $[M+3H]^{3+}$, found 1333.1.

Na_v and K_v channel constructs

Human (h)$Na_v1.4$, h$Na_v1.5$, and rat (r)$K_v2.1$ were generously provided by P. Ruben (Simon Fraser University, Canada), C. Ahern (University of Iowa, USA), and K. Swartz (NINDS, NIH, USA), respectively. h$Na_v1.1$–1.3, h$Na_v1.6$–1.8 were obtained from Origene Technologies, Inc. (MD, USA). Accession numbers are NM_001165963.1 (h$Na_v1.1$), NM_021007.2 (h$Na_v1.2$), NM_006922.3 (h$Na_v1.3$), NM_000334 (h$Na_v1.4$), NM_198056 (h$Na_v1.5$), NM_014191.2 (h$Na_v1.6$), NM_002977.2 (h$Na_v1.7$), and NM_006514.3 (h$Na_v1.8$). Channel chimeras were generated using sequential PCR with r$Na_v1.4$ (generous gift from B. Chanda, University of Wisconsin, USA), $K_v2.1\Delta7$[55,56], h$Na_v1.1$, and h$Na_v1.9$[24] (Origene Technologies: NM_014139.2) as templates. Mouse $K_v4.1$ was obtained from Addgene and originated in the laboratory of L. Salkoff. The $K_v2.1\Delta7$ construct contains seven point mutations in the outer vestibule that render the channel sensitive to agitoxin-2, a pore-blocking scorpion toxin[57]. cRNA of all constructs was synthesized using T3 or T7 polymerase (mMessage mMachine kit, Life Technologies, USA) after linearizing the fully-sequenced DNA with appropriate restriction enzymes.

Electrophysiology

Xenopus Oocytes— Channels and chimeras were expressed in *Xenopus laevis* oocytes (animals acquired from Xenopus one®, USA) that were incubated at 17 °C in Barth's medium (88 mM NaCl, 1 mM KCl, 0.33 mM $Ca(NO_3)_2$, 0.41 mM $CaCl_2$, 0.82 mM $MgSO_4$, 2.4 mM $NaHCO_3$, 5 mM HEPES, and 0.1 mg/mL gentamycin; pH 7.6 with NaOH) for 1–4 days after cRNA injection, and then were studied using two-electrode voltage-clamp recording techniques (OC-725C; Warner Instruments or GeneClamp 500B; Axon Instruments) with a 150-μl recording chamber or a small volume (<20μl) oocyte perfusion chamber (AutoMate Scientific). Data were filtered at 4 kHz and digitized at 20 kHz using pClamp 10 software (Molecular Devices, USA). Microelectrode resistances were 0.5–1 MΩ when filled with 3 M KCl. For K_v channel experiments, the external recording solution contained (in mM): 50 KCl, 50 NaCl, 5 HEPES, 1 $MgCl_2$ and 0.3 $CaCl_2$, pH 7.6 with

Author Manuscript Author Manuscript Author Manuscript Author Manuscript

NaOH. For Na_v channel experiments, the external recording solution contained (in mM): 100 NaCl, 5 HEPES, 1 $MgCl_2$ and 1.8 $CaCl_2$, pH 7.6 with NaOH. All experiments were performed at room temperature (~22 °C) and toxin samples were diluted in recording solution with 0.1% BSA. Leak and background conductance, identified by blocking the channel with agitoxin-2 or TTX, were subtracted for K_v or Na_v channel currents, respectively. Voltage–activation relationships were obtained by measuring tail currents for K_v channels, or by monitoring steady-state currents and calculating conductance for Na_v channels. Occupancy of closed or resting channels by toxins was examined using negative holding voltages where open probability was low, and the fraction of unbound channels was estimated using depolarizations that are too weak to open toxin-bound channels. After addition of toxin to the recording chamber, equilibration between toxin and channel was monitored using weak depolarizations elicited at 5–10 s intervals. For all channels, voltage–activation relationships were recorded in the absence and presence of toxin. Off-line data analysis was performed using Clampfit 10 (Molecular Devices, USA) and Origin 7.5 (Originlab, USA).

Multiple protocols were used to probe the biophysical characteristics of the Na_v channels and chimeras studied. To determine conductance-voltage and steady-state inactivation relationships, oocytes expressing Na_v channels were held at −90 mV and depolarized in 5 mV steps from −90 mV to 5 mV for 50 ms, immediately followed by a step to −15 mV to elicit the maximum available current and after 50 ms, returned to the −90 mV holding potential. Peak current generated during the incremental portion of the protocol was used to calculate the conductance-voltage relationship while the peak current during the −15 mV step as a function of the earlier voltage step was used to determine the steady-state inactivation relationship. The time constant of fast inactivation was determined by fitting single exponential curves to the −15 mV step of the aforementioned protocol. Boltzmann curves were fitted in Clampfit 10 (Molecular Devices, USA) and statistics calculated with Excel or the R statistical package (Student’s t-test).

Cultured neurons— Whole-cell patch clamp of cultured mouse TG neurons was performed as described[58]. Buffer solution contained (in mM) 150 NaCl, 2.8 KCl, 1 MgSO4, 10 HEPES, pH 7.4 (NaOH) and was perfused with or without toxins/drugs using a SmartSquirt Micro-Perfusion system (AutoMate). For colonic DRG, whole-cell recordings were made from fluorescently labeled thoracolumbar (T10-L1) colonic DRG neurons 20–48h after plating, using fire-polished glass electrodes with a resistance of 2–5 MΩ. All recordings were performed at room temperature (20–22°C). Signals were amplified by using an Axopatch 200A amplifier, digitized with a Digidata 1322A and recorded using pCLAMP 9 software (Molecular Devices, Sunnyvale, CA, USA). For all DRG neurons the holding potential was −70 mV. In current clamp mode a series of depolarizing pulses (500 ms, 10 pA step) were applied from holding potential (−70mV) and the rheobase (amount of current (pA) required for action potential generation) determined. The number of action potentials at 2x rheobase was also determined. Depolarizing pulses were tested in normal external bath solution and following the addition of Hm1a (100 nM). Control solutions and Hm1a were applied with a gravity driven multi-barrel perfusion system positioned within 1 mm of the neuron under investigation. Intracellular solutions contained (mM): 135 KCl; 2 $MgCl_2$; 2

Author Manuscript Author Manuscript Author Manuscript Author Manuscript

MgATP; 5 EGTA-Na; 10 HEPES-Na; adjusted to pH 7.4. Extracellular solutions contained (mM): 140 NaCl; 4 KCl; 2 $MgCl_2$; 2 $CaCl_2$; 10 HEPES-Na; 5 glucose; adjusted to pH 7.4.

Skin-nerve recordings— To assess primary afferent activity in response to the Hm1a spider toxin, we used the *ex vivo* skin-nerve preparation, as previously described[59]. Briefly, animals were lightly anesthetized via inhaled isoflurane and then killed via cervical dislocation. The hair on the lower extremities was shaved, and the hairy skin of the hindpaw was then quickly dissected along with its innervating saphenous nerve. The skin and nerve were then placed in a recording chamber filled with warmed (32° C), oxygenated buffer consisting of (in mM): 123 NaCl, 3.5 KCl, 2.0 CaCl2, 1.7 NaH2PO4, 0.7 MgSO4, 9.5 sodium gluconate, 5.5 glucose, 7.5 sucrose and 10 HEPES titrated to a pH of 7.45 ± 0.05.

The saphenous nerve was then threaded into a mineral oil-filled chamber, teased apart atop an elevated mirror plate, and placed on an extracellular recording electrode. Single unit receptive fields were then identified via a mechanical search stimulus using a blunt glass probe. Aδ afferents were identified based on a conduction velocity between 1.2 and 10 m/s, and were subtyped into A-mechanonociceptors (AMs) based on their slow adaptation to a mechanical stimulus[60].

After locating an AM fiber, to determine the threshold force for action potential generation, the receptive field was stimulated with calibrated Von Frey filaments. A metal moat (inner diameter: 4.7 mm) was then placed over the center of the receptive field to isolate it from the surrounding buffer. Buffer within the moat was then evacuated and replaced with a buffer containing either 1 μM Hm1a or vehicle (buffer). Receptive fields were incubated with toxin or buffer for 2–5 min. A custom-built, feedback-controlled mechanical stimulator was then placed within the moat and the receptive field was mechanically stimulated with a series of increasing forces (15 mN, 50 mN and 100 mN) for 10 seconds each. To avoid sensitization/desensitization, a rest period of 1 min was introduced between stimulations.

Data were digitized using a PowerLab A/D converter and recorded using LabChart software and Spike Histogram extension (AD Instruments, USA). All skin-nerve data were recorded and analyzed with the experimenter blinded to whether toxin or vehicle was used. Recordings were only included in the final data set if the firing of the fiber was clearly distinguishable from both background noise and any other fibers firing during stimulation.

Gut-nerve recordings— *Ex vivo* single-unit extracellular recordings of action potential discharge were made from splanchnic colonic afferents. Recordings were made from healthy or CVH mice using standard protocols [61–63]. Baseline mechanosensitivity was determined in response to application of a 2 g Von Frey hair (vfh) probe to the afferent receptive field for 3 seconds. This process was repeated 3–4 times, separated each time by 10 seconds. Mechanosensitivity was then re-tested after the application of Hm1a (100 nM) or the $Na_V1.1$ blocker ICA-121432 (500 nM) or a combination of both ICA-121432 (500 nM) and Hm1a (100 nM). Instantaneous frequency is defined as the inverse of the time interval between an action potential and the previous action potential. After application of Hm1a, significant increases ($p < 0.05$) in mechanically-evoked firing were seen overall in both healthy and CVH fibers. However, in both conditions we clearly recorded Hm1a-

Author Manuscript Author Manuscript Author Manuscript Author Manuscript

responsive and Hm1a-non-responsive neurons. We therefore binned fibers by responsiveness and present these data separately for clarity (Fig. 5 and Extended Data Fig. 5). Group data are presented as spikes/s and are expressed as mean ± SEM.

Animal use, husbandry and genotyping

Mice were bred and housed in accordance with UCSF Institutional Animal Care Committee (IACUC) guidelines. 2–5 animals were housed together with constant access to food and water. Floxed *SCN1A* mice[13] were generously provided by Dr. William Catterall (Department of Pharmacology, University of Washington). Floxed mice were bred to Peripherin–Cre (Per–Cre) mice[37] to produce *SCN1A*$^{F/F}$ x Per-Cre conditional knockout mice. $Na_v1.1$ floxed alleles were detected using primers previously described (Cheah) and Per-Cre expression was detected using the following primers to Cre recombinase: Cre_F: TAGCGTTCGAACGCACTGATTTCG; Cre_R: CGCCGTAAATCAATCGATGAGTTG.

Somatic behavioral experiments were approved by UCSF IACUC and were in accordance with the National Institutes of Health (NIH) Guide of the Care and Use of Laboratory Animals and the recommendation of the International Association for the Study of Pain. Animals used in skin-nerve recordings were naïve C57bl/6 male mice (n = 10), aged 6–16. Mice were housed on a 14:10 light:dark cycle with ad libitum access to food and water in a climate-controlled room. All protocols were approved by the Institutional Animal Care and Use Committee at the Medical College of Wisconsin. Animals used in colonic afferent and colonic DRG neuron studies were male C57BL/6J mice. The Animal Ethics Committees of The University of Adelaide and the South Australian Health and Medical Research Institute (SAHMRI) approved experiments involving animals.

Sensory neuron culture and calcium imaging

Trigeminal ganglia were dissected from newborn (P0–P3) Sprague-Dawley rats or C57BL/6 mice and cultured for >12 hours before calcium imaging or electrophysiological recording. Embryonic DRG cultures were generously provided by Jonah Chan[64]. Embryonic cultures were maintained as described and calcium imaging experiments were performed 1–10d after primary cultures were established. Primary cells were plated onto cover slips coated with poly-L-lysine (Sigma) and laminin (Invitrogen – 10μg/ml). Cells were loaded for calcium imaging with Fura-2-AM (Molecular Probes) for >1 h. Buffer solution – (in mM) 150 NaCl, 2.8 KCl, 1 MgSO4, 10 HEPES, pH 7.4 (NaOH) – was perfused with or without toxins/drugs using a SmartSquirt Micro-Perfusion system (AutoMate).

In situ hybridization and immunohistochemistry

In situ hybridization (ISH) was performed using the ViewRNA ISH Tissue 2-plex or 1-plex Assay Kits (Affymetrix). Target mRNA signals appear as puncta in bright field or fluorescent microscopy. Eight to twelve week old mice were deeply anesthetized with pentobarbital then transcardially perfused with 10 ml of phosphate buffered saline (PBS) followed by 10 ml of 10% neutral buffered formalin (NBF). DRGs were dissected, post-fixed in 10% NBF at 4°C O/N, cryoprotected in PBS with 30% w/v sucrose O/N at 4°C, then embedded in OCT Compound at −20°C. Tissue was sectioned at 12 μm, thaw-captured

Author Manuscript Author Manuscript Author Manuscript Author Manuscript

on Diamond White Glass slides (Globe Scientific), and stored at −20°C until use. Slides were used within two weeks of processing to produce optimal signals.

ViewRNA ISH Tissue 2-plex assay was performed with frozen tissue modifications as indicated by manufacturer including the endogenous alkaline phosphatase inactivation by incubation in H_2O with 0.1M HCl and 300 mM NaCl. H&E counterstaining procedure was omitted. Images were acquired with a Leica DMRB microscope and DFC500 digital camera using Leica Application Suite v3.5.0 then further analyzed using ImageJ software.

To co-label neuronal subpopulations markers (NF200, IB4, CGRP, TH) and $Na_v1.1$ mRNA, ViewRNA ISH Tissue 1-plex Assay and immunohistochemistry (IHC) were performed sequentially using a protocol modified from Ref. 65. ISH/IHC was not found to be compatible with all primary antibodies. Animals, tissue, and slides were prepared as described in the preceding paragraph. Frozen slides with tissue sections were warmed in a vacuum oven for 10 min at 60°C, fixed in PBS with 4% v/v formaldehyde for 10 min at room temperature (RT) then processed according to the manufacturer's protocol with frozen tissue modifications in a ThermoBrite Slide Processing System (Abbott Molecular). Washing steps were performed as indicated, in a deliberate and vigorous manner. Optimal protease and probe incubation times were determined to be 12 min and 2 h, respectively. Following development in Fast Red Substrate, slides were rinsed briefly in PBS then immediately processed for IHC. Slides were incubated for 1 h at RT in a blocking solution consisting of PBS with 0.1% v/v Triton X-100 (Sigma) and 10% normal goat serum (NGS). Slides were then incubated in primary antibody solution (PBS with 0.1% Triton X-100 and 2.5% NGS) overnight at 4°C, vigorously agitated for 2 min in fresh PBS 3X, then incubated in secondary antibody solution (PBS with 0.1% v/v Triton X-100) for 2 h at RT in the dark. Sections were then washed by vigorous agitation for 2 min in fresh PBS 3X prior to mounting with ProLong Gold antifade reagent with DAPI (Life Technologies) and coverslipping. Images were acquired with a Leica DMRB microscope and DFC500 digital camera using Leica Application Suite v3.5.0 then further analyzed using ImageJ software.

Affymetrix was commissioned to design a Type 1 probe set to mouse $Na_v1.1$ (*SCN1A*, NM_018733.2) and Type 6 probe sets to mouse TRPV1 (*TRPV1*, NM_001001445.2), mouse $Na_v1.7$ (*SCN9A*, NM_001290674.1), mouse $5HT_3$ (*HTR3A*, NM_001099644.1), and mouse TRPM8 (*TRPM8*, NM_134252.3) coding regions. We used the following primary antibodies: mouse anti-NF200 (1:10,000, Sigma), rabbit anti-CGRP (1:10,000, Peninsula Labs), and rabbit anti-TH (1:5,000, AbCam). We used fluorophore-conjugated secondary antibodies raised in goat against mouse or rabbit, as appropriate (1:1,000, Alexa Fluor 488, Life Technologies). To identify IB4-binding cells, biotinylated IB4 (1:1,000, Vector Labs) and fluorophore-conjugated streptavidin (1:1,000, Alexa Fluor 488, Life Technologies) were used in place of primary and secondary antibodies. Fos staining was performed 90 min after hindpaw injection of Hm1a or PBS. Spinal cord sections were prepared from lumbar L4/L5 and stained with rabbit anti-Fos (1:5,000, CalBiochem). ATF3 antibody (Santa Cruz Biotechnology) was used at 1:2000.

Author Manuscript Author Manuscript Author Manuscript Author Manuscript

Statistics and experimental design

Sample sizes for cellular physiology, histology and animal behavior were chosen based on previous experience with these assays as the minimum number of independent observation required for statistically significant results. For histology, at least three sections from each of at least three animals were counted. For oocyte and mouse neuron experiments, multiple batches/litters were used for all experiments. For behavioral experiments, animals were randomly chosen for different experimental cohorts by a blinded experimenter. Experimental and control conditions were compared within the same experimental time-course using randomly selected animals from one or multiple cages. Responses were then scored by an experimenter blinded to injection condition and experimental cohort. Animal genotype was tracked by ear tags and genotype unblinding occurred after analysis was complete.

Data were analyzed using Prism 6 software (GraphPad Software, San Diego, CA, USA) and significance testing used either Student's t-tests or one-way analysis of variance (ANOVA) followed by Bonferroni or Tukey's post-hoc tests, as noted in figure legends. All significance tests are two-sided. Significance levels are $*p < 0.05$, $**p < 0.01$, $***p < 0.001$, and $****p < 0.0001$. The number of experiments (n) and significance are reported in the figure legends. All significance tests were justified as appropriate given the experimental design and nature of the comparisons. We assume equal variance and normally distributed data within experimental paradigms where comparisons are made. These are common assumptions relied upon for significance testing within these experimental paradigms as previously published by our group and others.

Behavior

For behavioral experiments in Fig. 4, adult mice (6–12 weeks) were used. Male and female mice were first considered separately in hindpaw nocifensive response experiments. Both sexes showed significantly greater responses to toxin in WT littermate versus $Na_v1.1^{F/F}$ x Per-Cre CKO mice (one-sided unpaired Student's t test, $p < 0.05$, WT female: n = 5, CKO female: n = 6, WT male: n = 5, CKO male: n = 5). Therefore, male and female behavioral responses were pooled and subsequent experiments were performed on both male and female mice for CKO and WT littermate experiments, or only male mice for other conditions (e.g. Cap ablation). Nocifensive responses were recorded during a 20 min observation period immediately following intraplantar injections (10 μl PBS with or without 5 μM Hm1a). Licking/biting behavior was scored as seconds of behavior with the experimenter blinded to injection condition and experimental cohort (WT, CKO or Cap Ablated mice). Hargreaves and Von Frey tests were performed 30 min after intraplantar injection of 500 nM Hm1a or Hm1b to measure heat or mechanical sensitivity, respectively. Intrathecal (i.t.) cap ablation was performed as previously described[34], and i.t. cap treated mice were tested on a hot plate to ensure ablation of $TRPV1^+$ afferents. Ablation was also confirmed by histology.

Model of chronic visceral hypersensitivity

Colitis was induced by administration of 2,4,6-trinitrobenzenesulfonic acid (TNBS) as described previously[62,63]. Briefly, 13 week old anaesthetized mice were administered an intra-colonic enema of 0.1 mL TNBS (130 μg/mL in 30% ethanol) via a polyethylene

Author Manuscript Author Manuscript Author Manuscript Author Manuscript

catheter[62,63,66]. Histological examination of mucosal architecture, cellular infiltrate, crypt abscesses, and goblet cell depletion confirmed significant TNBS-induced damage by day 3 post-treatment, which largely recovered by day 7, and fully recovered by 28 days. High-threshold nociceptors from mice at the 28-day time point displayed significant mechanical hypersensitivity, lower mechanical activation thresholds, and hyperalgesia and allodynia[67]. As such, they are termed ‘chronic visceral hypersensitivity’ (CVH) mice[62,63,66,68].

Retrograde tracing and cell culture of colonic DRG neurons

Healthy and CVH mice of 16 weeks of age were anesthetized with halothane and following midline laparotomy, three 10 μL injections of the fluorescent retrograde neuronal tracer cholera toxin subunit B conjugated to AlexaFluor-488 were made sub-serosally within the wall of the descending colon. Four days after injection mice were sacrificed by CO_2 inhalation and DRGs from T10–L1 were surgically removed. DRGs were digested with 4 mg/mL collagenase II (GIBCO, Invitrogen) and 4 mg/mL dispase (GIBCO) for 30 min at 37°C, followed by 4 mg/mL collagenase II for 10 min at 37°C. Neurons were mechanically dissociated into a single-cell suspension via trituration through fire-polished Pasteur pipettes. Neurons were resuspended in DMEM (GIBCO) containing 10% FCS (Invitrogen), 2 mM L-glutamine (GIBCO), 100 μM MEM non-essential amino acids (GIBCO) and 100 mg/ml penicillin/streptomycin (Invitrogen). Neurons were spot-plated on 8 mm HCl treated coverslips coated with poly-D-lysine (800 μg/ml) and laminin (20 μg/ml) and maintained in an incubator at 37°C in 5% CO_2.

Author Manuscript Author Manuscript Author Manuscript Author Manuscript

Extended Data

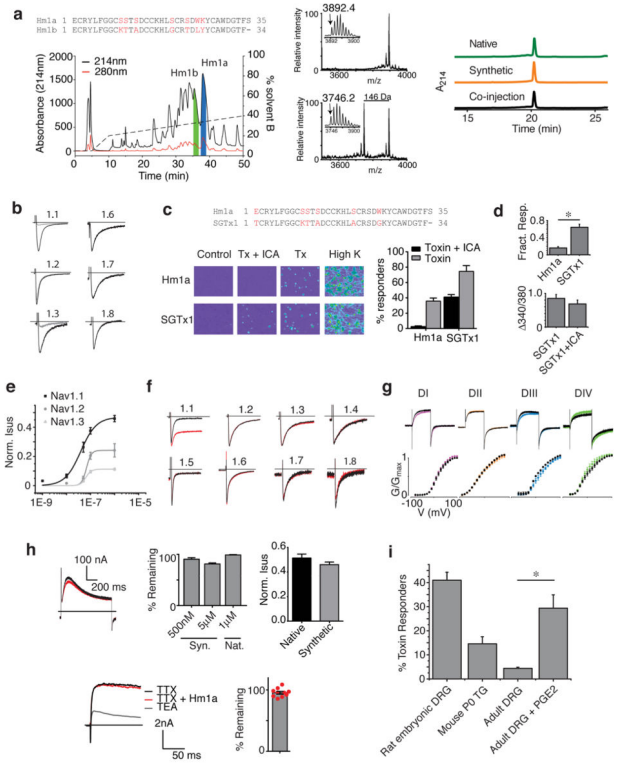

Extended Data Figure 1. Hm1a and 1b selectively target $Na_V1.1$ in sensory neurons

a, (Left) HPLC chromatogram showing reversed-phase C18 fractionation of *Heteroscodra maculata* venom; peaks containing Hm1a and Hm1b are labeled. Peptide sequences as determined by Edman degradation are displayed above. (Middle) MALDI-TOF spectra of native undigested Hm1b (top) and native Hm1b digested with carboxypeptidase Y for 20 min (bottom), with inserted spectra showing the monoisotopic mass of each in Dalton (Da). The observed mass difference of 146 Da between the intact and digested Hm1b corresponds to the final residue, Phe, with an amidated C-terminus. (Right) Chromatograms show reversed-phase C18 HPLC profiles of native and synthetic Hm1a, which were indistinguishable when co-injected. **b**, Representative currents from oocytes expressing hNa_V subtypes before (black) and after (grey) bath application of ICA-121431 (500 nM). Currents were elicited during 1 Hz stimulation to induce use-dependent block. **c**, (Top) Amino acid sequence comparison of Hm1a with SGTx1, a related, but non-selective fast-inactivation inhibitor. (Bottom) Representative calcium imaging experiment comparing ICA-121431-mediated block of Hm1a- or SGTx1-evoked responses in cultured embryonic DRG neurons, with group data at right (**$p < 0.01$, ***$p < 0.001$, n = 4). **d**, (Top) Fraction of P0 mouse neurons responding to Hm1a versus SGTx1 (**$p < 0.01$). (Bottom) Ratiometric calcium responses elicited by SGTx1 (500 nM) in the presence and absence of ICA-121431 (500 nM). **e**, Dose-response curves for Hm1a inhibition of fast inactivation in oocytes expressing $Na_V1.1$, $Na_V1.2$ or $Na_V1.3$. Sustained current at the end of a 100 ms pulse is normalized to peak current to quantify magnitude of the effect. EC_{50} for $hNa_V1.1$ = 38 nM, $hNa_V1.2$ = 236 nM and $hNa_V1.3$ = 220 nM. **f**, Representative traces from oocytes expressing hNa_V subtypes

Author Manuscript Author Manuscript Author Manuscript Author Manuscript

in response to a saturating dose (on $hNa_v1.1$) of purified Hm1b during a 100 ms depolarization. **g**, $rK_v2.1$ chimeras containing different $Na_v1.9$ S3b-S4 motifs were tested for sensitivity to hHm1a (100 nM). Representative traces (top) and summary data (bottom) show a lack of toxin sensitivity for each chimera. **h**, (Top left) Representative currents from oocytes expressing $mK_v4.1$ before (black) and after (red) bath application of Hm1a (5 μM). (Middle) Quantification of $mK_v4.1$ blockade by synthetic or native Hm1a. (Top right) Comparison of sustained current during application of native or synthetic Hm1a (1 μM) shows similar effects on $Na_v1.1$ inactivation. (Bottom) Representative traces (left) showing that outward currents in P0 TG mouse neurons are unaffected by Hm1a (500 nM). Scatter plot (right, n = 10) shows no significant difference). **i**, Percentage of Hm1a (500 nM)-responsive neurons in various culture conditions as assessed by calcium imaging (n = 3–4,* $p < 0.05$).

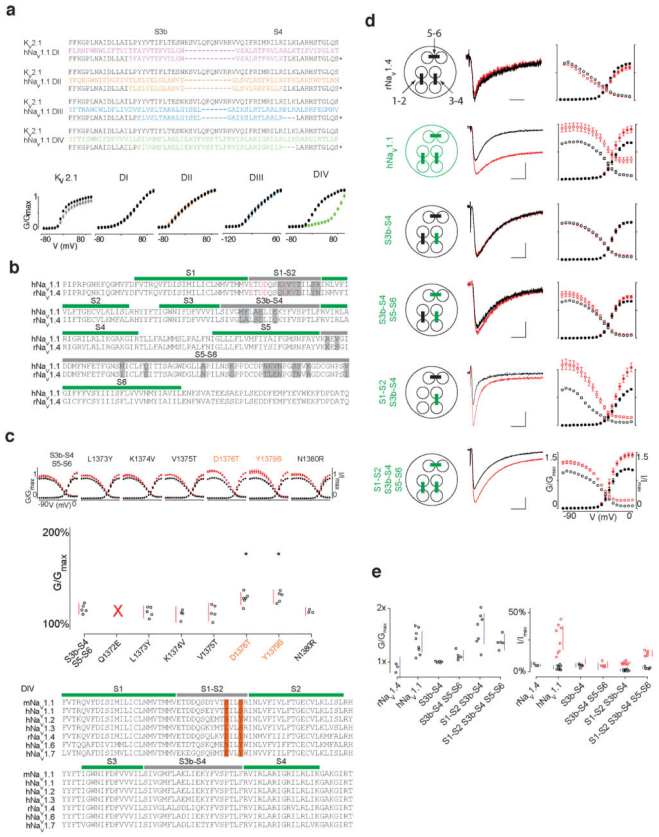

Extended Data Figure 2. Hm1a selectivity depends on DIV S1-S2 and S3b-S4 regions

a, (Top) Alignments between $K_v2.1$ and $hNa_v1.1$ S3b-S4 regions from each domain (as indicated) with sequence of chimeras shown below each alignment. (Bottom) G-V relationships from chimeric channels expressed in oocytes in the absence (black) and presence (colors) of Hm1a (100 nM). **b**, Sequence alignment of $hNa_v1.1$ and $rNa_v1.4$ showing putative transmembrane segments (green) and regions swapped in chimeric channels (grey). **c**, (Top) Using the background of $Na_v1.4$ chimera containing the S3b-S4 and S5-S6 regions of $Na_v1.1$, individual residues were mutated in the S1-S2 loop to the cognate residue in $Na_v1.1$. The D1376T and Y1379S point mutants in the chimeric $rNa_v1.4$

Author Manuscript Author Manuscript Author Manuscript Author Manuscript

channel reveal an increase in peak current after 100 nM Hm1a application (red) relative to untreated controls (black). Filled circles denote G-V relationships, where oocytes were depolarized for 50 ms in 5mV steps from a holding potential of −90mV. Open circles denote steady-state inactivation (I/Imax) relationships, where oocytes were depolarized from −90mV to +5mV in 5mV increments for 50 ms preceeding a 50 ms step to −15mV. (Middle) Dot plot detailing percent increase in peak conductance of each point mutant in response to 100 nM Hm1a treatment. Each point represents a single oocyte; red bars indicate 95% confidence interval. Mutations highlighted in orange (D1376T and Y1379S) are statistically different from S3b-S4/S5-S6 control (*$p < 0.01$). The Q1372E mutant did not generate currents. (Bottom) Alignment of DIV S1-S4 regions from relevant mouse and human Na_v isoforms. Orange highlights location of residues in the S1-S2 loop that putatively contribute to the toxin effect. **d**, (Left) Stylized DIV with transmembrane segments represented as circles and extracellular loops as bars (black for native rNa_v1.4 channel and green for portions transplanted from hNa_v1.1). (Middle) Traces displaying effect of Hm1a on each chimera depolarized to −15 mV from a holding potential of −90 mV. (Right) Conductance-voltage (G/Gmax) and steady-state inactivation (I/Imax) relationships of each channel and chimera before and after toxin (black and red, respectively) across a voltage range spanning −90 mV to 0 mV from a holding potential of −90 mV in 5 mV increments. Scale bars as in Fig. 2. **e**, Dot plots displaying the effect of 100 nM Hm1a on peak current (left) and persistent current (right). Data in the left plot were generated by dividing peak conductance after Hm1a application by the peak conductance before. Right plot shows persistent current divided by peak current before (black) or after (red) toxin addition. Persistent current was determined by averaging current from the final millisecond of depolarization to 0 mV from a holding potential of −90 mV. Vertical bars indicate 95% confidence interval.

Author Manuscript Author Manuscript Author Manuscript Author Manuscript

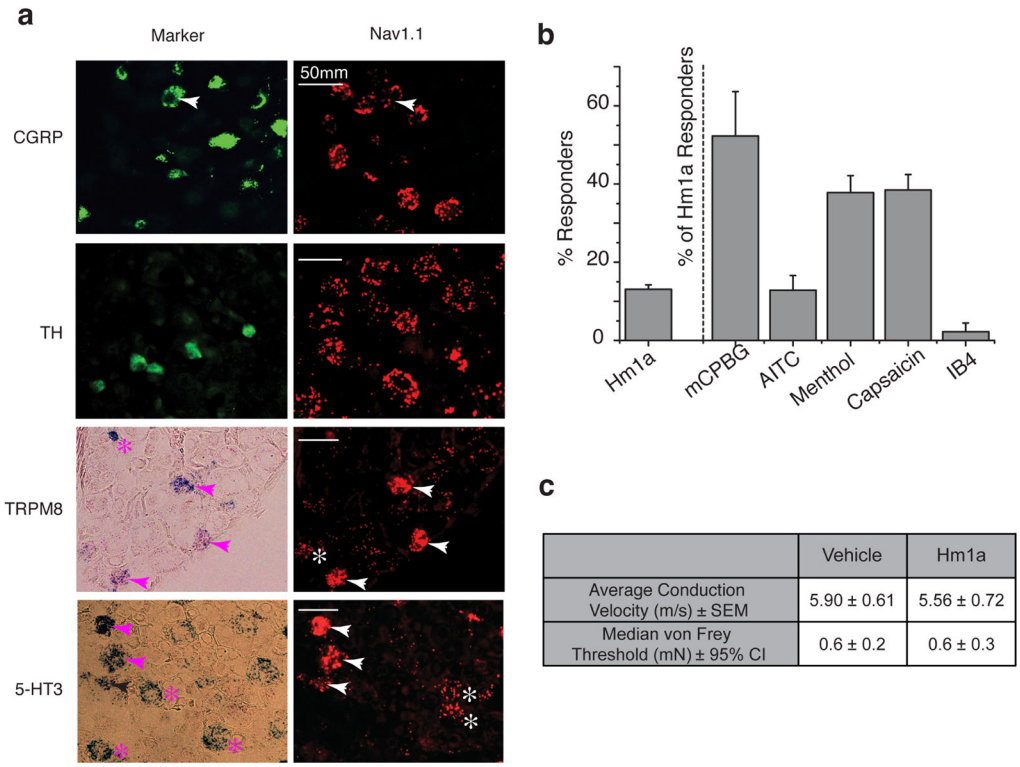

c

	Vehicle	Hm1a
Average Conduction Velocity (m/s) ± SEM	5.90 ± 0.61	5.56 ± 0.72
Median von Frey Threshold (mN) ± 95% CI	0.6 ± 0.2	0.6 ± 0.3

Extended Data Figure 3. $Na_v1.1$ is expressed by myelinated, non-C fiber sensory neurons

a, Representative images showing expression of various molecular markers and their overlap with $Na_v1.1$ transcripts. Markers include immunohistochemical staining for calcitonin gene related peptide (CGRP) and tyrosine hydroxylase (TH) and *in situ* histochemistry for TRPM8 and 5-HT_3 ion channel transcripts, Quantification of overlap for these markers is shown in Fig. 3. **b**, Quantification of the number of toxin-responsive cells in P0 mouse TG cultures as assessed by calcium imaging (leftmost column) and the percentage of toxin-sensitive cells that responded to other agonists (mCPBG, AITC, capsaicin, and menthol activate 5-HT_3, TRPA1, TRPV1 and TRPM8 channels, respectively), or bound the lectin IB4. **c**, Table including conduction velocity and Von Frey thresholds for skin-nerve experiments presented in Fig. 3d.

Author Manuscript Author Manuscript Author Manuscript Author Manuscript

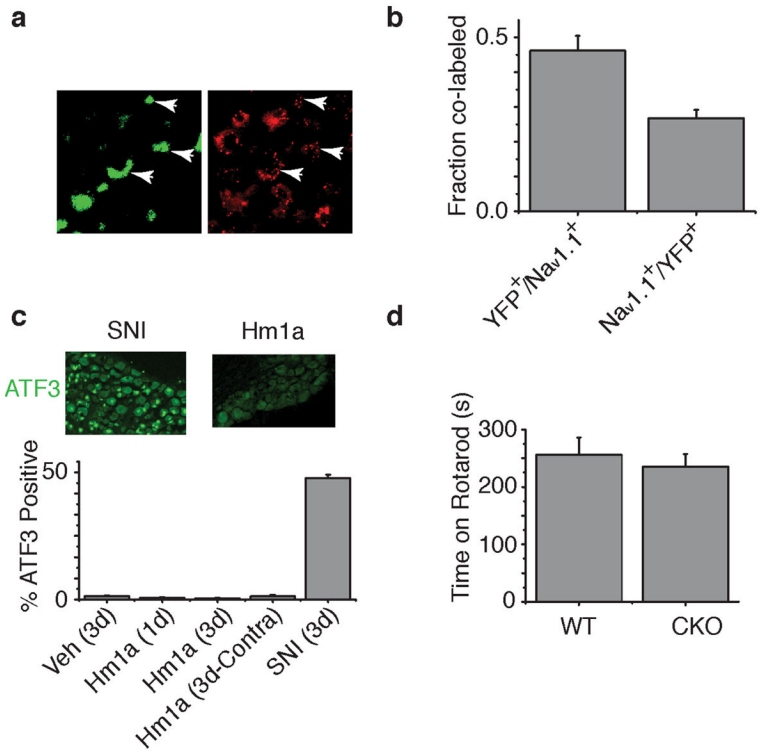

Extended Data Figure 4. Control experiments related to Figure 4

a, Representative DRG sections from peripherin-Cre adult mouse showing neurons that express Cre recombinase as visualized using a floxed-stop YFP reporter mouse. *In situ* hybridization histochemistry shows overlap with $Na_V1.1$ transcripts (right panel). **b**, Quantification of overlap between YFP and $Na_V1.1$. **c**, Comparison of ATF3 induction in DRG following sciatic nerve ligation (SNI) or intraplantar Hm1a injection. SNI induced ATF3 expression in >50% of DRG neurons whereas ATF3 induction after Hm1a injection was indistinguishable from vehicle (measured 1 or 3 days post-injection). **d**, Peripherin-Cre x floxed $Na_V1.1$ mice were compared with WT littermates in the rotarod test. No significant differences were observed.

Author Manuscript Author Manuscript Author Manuscript Author Manuscript

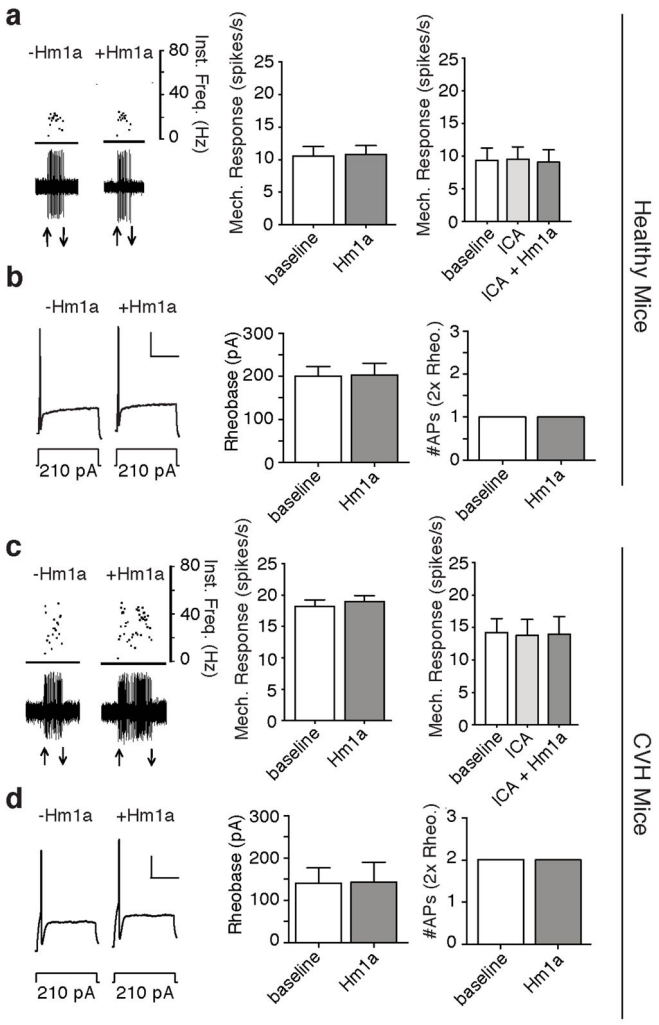

Extended Data Figure 5. A subset of colonic afferents does not express functional $Na_V1.1$

a, (Left) Representative *ex vivo* colonic single fiber recording from an Hm1a (100 nM)-non-responsive high-threshold fiber from a healthy mouse (arrows indicate application and removal of 2g Von Frey hair stimulus). (Middle) Group data showing lack of Hm1a-mediated responses from a subset (9/15) of fibers. (Right) Group data showing a population (5/10) of healthy, high-threshold mechanoreceptor colonic afferents unaltered by ICA-121432 either in the presence or absence of Hm1a (100 nM). **b,** (Left) Representative whole–cell current clamp recording of a retrogradely traced colonic DRG neuron in response to 500 ms current injection at rheobase. Recordings were made from the same neuron of a healthy control mouse before and after incubation with Hm1a (10 nM). Horizontal scale bar = 250 ms; vertical scale bar = 20 mV. (Middle and Right) Group data show no effect from Hm1a application on electrical excitability in a sub-population (6/11) of colonic DRG neurons. **c,** (Left) Representative high-threshold mechanoreceptive colonic fibers from CVH mice showing no change after application of Hm1a (100 nM). (Middle) Group data from Hm1a-non-responsive colonic fibers (4/11). (Right) Group data showing a subpopulation of CVH colonic afferents (3/10) unaltered by ICA-121432 either in the

Author Manuscript Author Manuscript Author Manuscript Author Manuscript

presence or absence of Hm1a. **d,** (Left) Representative Hm1a-non-responsive colonic DRG neuron in whole-cell current clamp. (Middle and Left) Group data show electrical excitability is unaltered by Hm1a in a subset (4/11) of CVH colonic DRG neurons.

Supplementary Material

Refer to Web version on PubMed Central for supplementary material.

Acknowledgments

We thank the Deutsche Arachnologische Gesellschaft and particularly I. Wendt, J. Broghammer, A. Schlosser, B. Rast, M. Luescher, C. Schneider and H. Auer for providing arthropods for milking, Dr. William Catterall for providing floxed Nav1.1 mice, and J. Poblete, J. Maddern, T. O'Donnell and A. Harrington for technical assistance. This work was supported by Ruth Kirschstein NIH postdoctoral (F32NS081907 to J.D.O.) and predoctoral (F31NS084646 to J.G. and F30DE023476 to J.J.E.) fellowships, the National Institutes of Health (R37NS065071 and R01NS081115 to D.J., R01NS091352 to F.B., R01NS040538 and R01NS070711 to C.L.S., and R37NS014627 and R01DA29204 to A.I.B.), the National Health and Medical Research Council of Australia (Project Grant #APP1083480 to S.M.B., Program Grant APP1072113 and Principal Research Fellowship APP1044414 to G.F.K.), and a grant from the Wellcome Trust to A.I.B. S.M.B. is a NHMRC R.D Wright Biomedical Research Fellow.

References

1. Basbaum AI, Bautista DM, Scherrer G, Julius D. Cellular and molecular mechanisms of pain. Cell. 2009; 139:267–284. [PubMed: 19837031]
2. Dib-Hajj SD, Yang Y, Black JA, Waxman SG. The $Na_V1.7$ sodium channel: from molecule to man. Nat Rev Neurosci. 2013; 14:49–62. [PubMed: 23232607]
3. Faber CG, et al. Gain-of-function $Na_V1.8$ mutations in painful neuropathy. Proc Natl Acad Sci U S A. 2012; 109:19444–19449. [PubMed: 23115331]
4. Fertleman CR, et al. SCN9A mutations in paroxysmal extreme pain disorder: allelic variants underlie distinct channel defects and phenotypes. Neuron. 2006; 52:767–774. [PubMed: 17145499]
5. Hoeijmakers JG, Faber CG, Merkies IS, Waxman SG. Painful peripheral neuropathy and sodium channel mutations. Neurosci Lett. 2015; 596:51–59. [PubMed: 25556685]
6. Zhang XY, et al. Gain-of-function mutations in *SCN11A* cause familial episodic pain. Am J Hum Genet. 2013; 93:957–966. [PubMed: 24207120]
7. Fukuoka T, et al. Comparative study of the distribution of the α-subunits of voltage-gated sodium channels in normal and axotomized rat dorsal root ganglion neurons. J Comp Neurol. 2008:510.
8. Black JA, Liu SJ, Tanaka M, Cummins TR, Waxman SG. Changes in the expression of tetrodotoxin-sensitive sodium channels within dorsal root ganglia neurons in inflammatory pain. Pain. 2004:108. [PubMed: 15109513]
9. Fukuoka T, Miyoshi K, Noguchi K. De novo expression of Nav1.7 in injured putative proprioceptive afferents: multiple tetrodotoxin-sensitive sodium channels are retained in the rat dorsal root after spinal nerve ligation. Neuroscience. 2015; 284:693–706. [PubMed: 25453779]
10. Dib-Hajj SD, Cummins TR, Black JA, Waxman SG. Sodium channels in normal and pathological pain. Annu Rev Neurosci. 2010; 33:325–347. [PubMed: 20367448]
11. Wang W, Gu J, Li YQ, Tao YX. Are voltage-gated sodium channels on the dorsal root ganglion involved in the development of neuropathic pain? Mol Pain. 2011; 7:16. [PubMed: 21345196]
12. Catterall WA, Kalume F, Oakley JC. $Na_V1.1$ channels and epilepsy. J Physiol. 2010; 588:1849–1859. [PubMed: 20194124]
13. Cheah CS, et al. Specific deletion of $Na_V1.1$ sodium channels in inhibitory interneurons causes seizures and premature death in a mouse model of Dravet syndrome. Proc Natl Acad Sci U S A. 2012; 109:14646–14651. [PubMed: 22908258]
14. Han S, et al. Autistic-like behaviour in *Scn1a*$^{+/-}$ mice and rescue by enhanced GABA-mediated neurotransmission. Nature. 2012; 489:385–390. [PubMed: 22914087]

Author Manuscript Author Manuscript Author Manuscript Author Manuscript

15. Verret L, et al. Inhibitory interneuron deficit links altered network activity and cognitive dysfunction in Alzheimer model. Cell. 2012; 149:708–721. [PubMed: 22541439]
16. Gargus JJ, Tournay A. Novel mutation confirms seizure locus SCN1A is also familial hemiplegic migraine locus FHM3. Pediatr Neurol. 2007; 37:407–410. [PubMed: 18021921]
17. Cestele S, Schiavon E, Rusconi R, Franceschetti S, Mantegazza M. Nonfunctional $Na_V1.1$ familial hemiplegic migraine mutant transformed into gain of function by partial rescue of folding defects. Proc Natl Acad Sci U S A. 2013; 110:17546–17551. [PubMed: 24101488]
18. Priest BT. Future potential and status of selective sodium channel blockers for the treatment of pain. Curr Opin Drug Discov Devel. 2009; 12:682–692.
19. Bohlen CJ, Julius D. Receptor-targeting mechanisms of pain-causing toxins: How ow? Toxicon. 2012; 60:254–264. [PubMed: 22538196]
20. Olivera BM, Hillyard DR, Marsh M, Yoshikami D. Combinatorial peptide libraries in drug design: lessons from venomous cone snails. Trends Biotechnol. 1995; 13:422–426. [PubMed: 7546566]
21. Black JA, et al. Spinal sensory neurons express multiple sodium channel α-subunit mRNAs. Brain Res Mol Brain Res. 1996; 43:117–131. [PubMed: 9037525]
22. McCormack K, et al. Voltage sensor interaction site for selective small molecule inhibitors of voltage-gated sodium channels. Proc Natl Acad Sci U S A. 2013; 110:E2724–2732. [PubMed: 23818614]
23. Bosmans F, Martin-Eauclaire MF, Swartz KJ. Deconstructing voltage sensor function and pharmacology in sodium channels. Nature. 2008; 456:202–208. [PubMed: 19005548]
24. Bosmans F, Puopolo M, Martin-Eauclaire MF, Bean BP, Swartz KJ. Functional properties and toxin pharmacology of a dorsal root ganglion sodium channel viewed through its voltage sensors. J Gen Physiol. 2011; 138:59–72. [PubMed: 21670206]
25. Escoubas P, Diochot S, Celerier ML, Nakajima T, Lazdunski M. Novel tarantula toxins for subtypes of voltage-dependent potassium channels in the Kv2 and Kv4 subfamilies. Mol Pharmacol. 2002; 62:48–57. [PubMed: 12065754]
26. Smith JAM, Davis CL, Burgess GM. Prostaglandin E-2-induced sensitization of bradykinin-evoked responses in rat dorsal root ganglion neurons is mediated by cAMP-dependent protein kinase A. Eur J Neurosci. 2000; 12:3250–3258. [PubMed: 10998108]
27. Wang J, et al. Mapping the receptor site for α-scorpion toxins on a Na^+ channel voltage sensor. Proc Natl Acad Sci U S A. 2011; 108:15426–15431. [PubMed: 21876146]
28. Bende NS, et al. A distinct sodium channel voltage-sensor locus determines insect selectivity of the spider toxin Dc1a. Nat Commun. 2014; 5:4350. [PubMed: 25014760]
29. Zeitz KP, et al. The 5-HT3 subtype of serotonin receptor contributes to nociceptive processing via a novel subset of myelinated and unmyelinated nociceptors. J Neurosci. 2002; 22:1010–1019. [PubMed: 11826129]
30. Bautista DM, et al. The menthol receptor TRPM8 is the principal detector of environmental cold. Nature. 2007; 448:204–208. [PubMed: 17538622]
31. Usoskin D, et al. Unbiased classification of sensory neuron types by large-scale single-cell RNA sequencing. Nat Neurosci. 2015; 18:145–153. [PubMed: 25420068]
32. Cavanaugh DJ, et al. Restriction of transient receptor potential vanilloid-1 to the peptidergic subset of primary afferent neurons follows its developmental downregulation in nonpeptidergic neurons. J Neurosci. 2011; 31:10119–10127. [PubMed: 21752988]
33. Stucky CL, Medler KA, Molliver DC. The P2Y agonist UTP activates cutaneous afferent fibers. Pain. 2004; 109:36–44. [PubMed: 15082124]
34. Cavanaugh DJ, et al. Distinct subsets of unmyelinated primary sensory fibers mediate behavioral responses to noxious thermal and mechanical stimuli. Proc Natl Acad Sci U S A. 2009; 106:9075–9080. [PubMed: 19451647]
35. Mishra SK, Tisel SM, Orestes P, Bhangoo SK, Hoon MA. TRPV1-lineage neurons are required for thermal sensation. EMBO J. 2011; 30:582–593. [PubMed: 21139565]
36. Mishra SK, Hoon MA. Ablation of TrpV1 neurons reveals their selective role in thermal pain sensation. Mol Cell Neurosci. 2010; 43:157–163. [PubMed: 19853036]

Author Manuscript Author Manuscript Author Manuscript Author Manuscript

37. Scherrer G, et al. VGLUT2 expression in primary afferent neurons is essential for normal acute pain and injury-induced heat hypersensitivity. Proc Natl Acad Sci USA. 2010; 107:22296–22301. [PubMed: 21135246]
38. Koltzenburg M, Wall PD, McMahon SB. Does the right side know what the left is doing? Trends Neurosci. 1999; 22:122–127. [PubMed: 10199637]
39. Kissin I, Lee SS, Bradley EL. Effect of prolonged nerve block on inflammatory hyperalgesia in rats — prevention of late hyperalgesia. Anesthesiology. 1998; 88:224–232. [PubMed: 9447876]
40. Tsujino H, et al. Activating transcription factor 3 (ATF3) induction by axotomy in sensory and motoneurons: A novel neuronal marker of nerve injury. Mol Cell Neurosci. 2000; 15:170–182. [PubMed: 10673325]
41. Brierley SM, Linden DR. Neuroplasticity and dysfunction after gastrointestinal inflammation. Nat Rev Gastroenterol Hepatol. 2014; 11:611–627. [PubMed: 25001973]
42. de Araujo AD, et al. Selenoether oxytocin analogues have analgesic properties in a mouse model of chronic abdominal pain. Nat Commun. 2014; 5 ARTN 3165.
43. Jensen HS, Grunnet M, Bastlund JF. Therapeutic potential of $Na_V1.1$ activators. Trends Pharmacol Sci. 2014; 35:113–118. DOI: 10.1016/j.tips.2013.12.007 [PubMed: 24439681]
44. Khan GM, Chen SR, Pan HL. Role of primary afferent nerves in allodynia caused by diabetic neuropathy in rats. Neuroscience. 2002; 114:291–299. [PubMed: 12204199]
45. Tsunozaki M, et al. A 'toothache tree' alkylamide inhibits Aδ mechanonociceptors to alleviate mechanical pain. J Physiol-London. 2013; 591:3325–3340. [PubMed: 23652591]
46. Pappagallo M. Newer antiepileptic drugs: possible uses in the treatment of neuropathic pain and migraine. Clin Ther. 2003; 25:2506–2538. [PubMed: 14667954]
47. Calabresi P, Galletti F, Rossi C, Sarchielli P, Cupini LM. Antiepileptic drugs in migraine: from clinical aspects to cellular mechanisms. Trends Pharmacol Sci. 2007; 28:188–195. [PubMed: 17337068]
48. Gilchrist J, et al. $Na_V1.1$ modulation by a novel triazole compound attenuates epileptic seizures in rodents. ACS Chem Biol. 2014; 9:1204–1212. [PubMed: 24635129]
49. Suter MR, Kirschmann G, Laedermann CJ, Abriel H, Decosterd I. Rufinamide attenuates mechanical allodynia in a model of neuropathic pain in the mouse and stabilizes voltage-gated sodium channel inactivated state. Anesthesiology. 2013; 118:160–172. [PubMed: 23221868]
50. Herzig V, et al. ArachnoServer 2.0, an updated online resource for spider toxin sequences and structures. Nucleic Acids Res. 2011; 39:D653–657. [PubMed: 21036864]
51. Chow CY, Cristofori-Armstrong B, Undheim EAB, King GF, Rash LD. Three peptide modulators of the human voltage-gated sodium channel 1.7, an important analgesic target, from the venom of an Australian tarantula. Toxins. 2015; 7:2494–2513. [PubMed: 26134258]
52. Kamber B, et al. The synthesis of cystine peptides by iodine oxidation of *S*-trityl-cysteine and *S*-acetamidomethyl-cysteine peptides. Helv Chim Acta. 1980; 63:899–915.
53. Vetter I, et al. Isolation, characterization and total regioselective synthesis of the novel μO-conotoxin MfVIA from *Conus magnificus* that targets voltage-gated sodium channels. Biochem Pharmacol. 2012; 84:540–548. [PubMed: 22609441]
54. Gongora-Benitez M, et al. Acid-labile Cys-protecting groups for the Fmoc/tBu Strategy: filling the gap. Org Lett. 2012; 14:5472–5475. [PubMed: 23075170]
55. Frech GC, VanDongen AM, Schuster G, Brown AM, Joho RH. A novel potassium channel with delayed rectifier properties isolated from rat brain by expression cloning. Nature. 1989; 340:642–645. [PubMed: 2770868]
56. Swartz KJ, MacKinnon R. Hanatoxin modifies the gating of a voltage-dependent K^+ channel through multiple binding sites. Neuron. 1997; 18:665–673. [PubMed: 9136774]
57. Garcia ML, Garcia-Calvo M, Hidalgo P, Lee A, MacKinnon R. Purification and characterization of three inhibitors of voltage-dependent K^+ channels from *Leiurus quinquestriatus* var. *hebraeus* venom. Biochemistry. 1994; 33:6834–6839. [PubMed: 8204618]
58. Bohlen CJ, et al. A bivalent tarantula toxin activates the capsaicin receptor, TRPV1, by targeting the outer pore domain. Cell. 2010; 141:834–845. [PubMed: 20510930]

Author Manuscript Author Manuscript Author Manuscript Author Manuscript

59. Reeh PW. Sensory receptors in mammalian skin in an in vitro preparation. Neurosci Lett. 1986; 66:141–146. [PubMed: 3725179]

60. Koltzenburg M, Stucky CL, Lewin GR. Receptive properties of mouse sensory neurons innervating hairy skin. J Neurophysiol. 1997; 78:1841–1850. [PubMed: 9325353]

61. Brierley SM, Jones RC III, Gebhart GF, Blackshaw LA. Splanchnic and pelvic mechanosensory afferents signal different qualities of colonic stimuli in mice. Gastroenterology. 2004; 127:166–178. [PubMed: 15236183]

62. Castro J, et al. Linaclotide inhibits colonic nociceptors and relieves abdominal pain via guanylate cyclase-C and extracellular cyclic guanosine 3′,5′-monophosphate. Gastroenterology. 2013; 145:1334–1346. e1331–1311. [PubMed: 23958540]

63. de Araujo AD, et al. Selenoether oxytocin analogues have analgesic properties in a mouse model of chronic abdominal pain. Nat Commun. 2014; 5:3165. [PubMed: 24476666]

64. Lewallen KA, et al. Assessing the role of the cadherin/catenin complex at the Schwann cell-axon interface and in the initiation of myelination. J Neurosci. 2011; 31:3032–3043. [PubMed: 21414924]

65. Bardoni R, et al. Delta opioid receptors presynaptically regulate cutaneous mechanosensory neuron input to the spinal cord dorsal horn. Neuron. 2014; 81:1312–1327. [PubMed: 24583022]

66. Hughes PA, et al. Post-inflammatory colonic afferent sensitisation: different subtypes, different pathways and different time courses. Gut. 2009; 58:1333–1341. [PubMed: 19324867]

67. Brierley SM, Linden DR. Neuroplasticity and dysfunction after gastrointestinal inflammation. Nat Rev Gastroenterol Hepatol. Oct.2014 11:611–627. [PubMed: 25001973]

68. Hughes PA, et al. Increased κ-opioid receptor expression and function during chronic visceral hypersensitivity. Gut. 2014; 63:1199–1200. [PubMed: 24285775]

Author Manuscript Author Manuscript Author Manuscript Author Manuscript

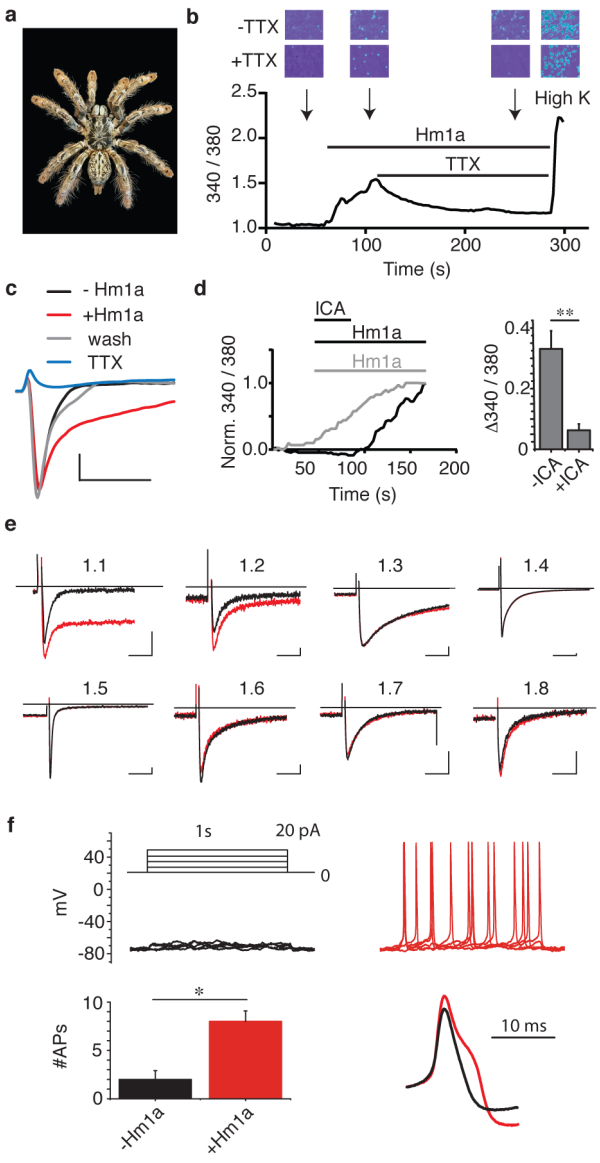

Figure 1. Hm1a selectively targets $Na_v1.1$ in sensory neurons

a, Togo Starburst tarantula, *H. maculata* (image courtesy of B. Rast, ArachnoServer [50]). **b**, Average ratiometric calcium responses from Hm1a (500nM)-sensitive embryonic rat DRG neurons with or without TTX (500 nM). Note persistence of toxin responses in the absence of TTX (top images). **c**, Representative whole-cell patch clamp recording from Hm1a-sensitive P0 mouse TG neuron. All (15/15) Hm1a responsive neurons displayed similar effect of toxin on sodium current inactivation. Currents elicited during repeated steps to −30 mV (V_h = −90 mV, scale bar = 1nA, 5ms). **d**, (Left) Average Hm1a-evoked calcium response in the presence of ICA-121431 (500nM) and after washout (n = 11; responses to Hm1a alone are shown in grey). (Right) Quantification of maximum Hm1a-evoked responses with or without ICA-121431 (n = 25). **e**, Currents from oocytes expressing hNa_v channels in the absence (black) or presence (red, 100nM) of Hm1a elicited by repeated pulses (0.2–1Hz) to −30mV ($Na_v1.1$–1.7) or 0 mV ($Na_v1.8$) for 100ms (V_h = −90mV). Scale

bar = 100nA, 25ms. **f**, (Top panels) Representative current clamp recording from mouse TG neuron in the absence (black) or presence (red) of Hm1a (500nM). (Bottom) Quantification of action potentials (APs) elicited by a 1s, 20pA current injection before or after exposure to Hm1a (500nM, n = 4) with representative APs shown at right. Average AP width increased in the presence of Hm1a by 28.3% ± 8.4% ($p < 0.05$, n = 4). *$p < 0.05$ and ***$p < 0.001$, Student's t-test. Error bars represent mean ± SEM.

Author Manuscript Author Manuscript Author Manuscript Author Manuscript

Author Manuscript Author Manuscript Author Manuscript Author Manuscript

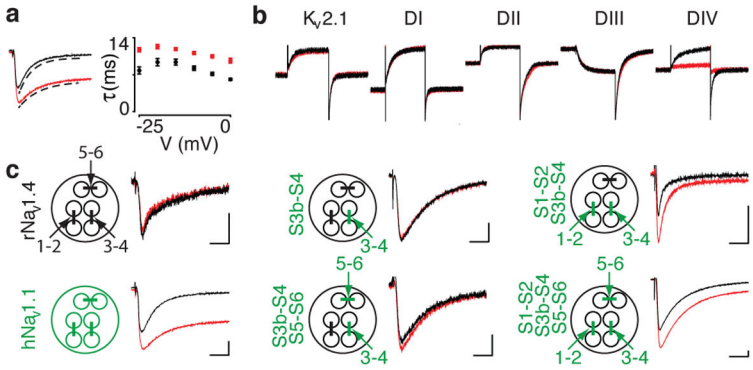

Figure 2. Hm1a targets S3b-S4 and S1-S2 loops in DIV to inhibit fast inactivation

a, Representative traces from oocytes expressing hNa$_v$1.1 without (black) or with (red) Hm1a (100nM). Single exponential fits to inactivation time course (broken lines) and tau values (right) show toxin-induced slowing (** $p < 0.01$ at each voltage, 2-way ANOVA with post-hoc Tukey's). **b**, K_v2.1 (far left) and chimeras containing S3b-S4 motif from each hNa$_v$1.1 domain repeat (DI-DIV, as indicated) were tested for sensitivity to Hm1a (100nM). Currents are shown during 50ms depolarization to −30mV. Scale bar = 200nA; 10ms. **c**, rNa$_v$1.4, hNa$_v$1.1 and chimeric channels containing S1-S2, S3b-S4, and/or S5-S6 were tested for Hm1a sensitivity. See Extended Data Figure 2 for quantitation and details of chimera design.

Author Manuscript Author Manuscript Author Manuscript Author Manuscript

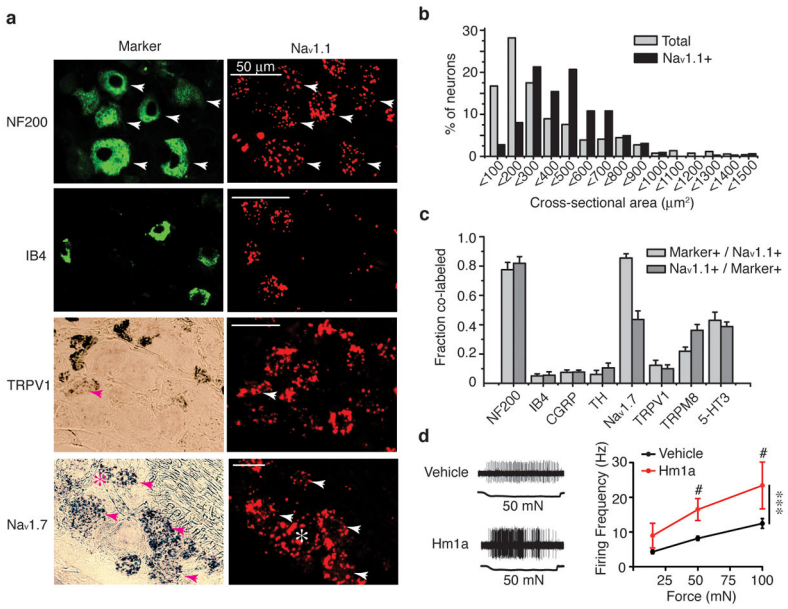

Figure 3. $Na_V1.1$ is expressed by myelinated, non-C fiber neurons in sensory ganglia

a, Representative DRG sections showing immunoreactivity for neurofilament 200 (NF200), binding of isolectin B4 (IB4), and *in situ* histochemistry for TRPV1, $Na_V1.7$, or $Na_V1.1$ transcripts, as indicated. Arrows and asterisks indicate cells with overlapping and non-overlapping signals, respectively. **b**, Size distribution for all DRG neurons (grey bars, 514 cells counted) or $Na_V1.1$-expressing cells (black bars, 324 cells counted). **c**, Quantification of overlap between histological markers (≥164 cells counted for each condition; 9–12 independent sections from ≥3 mice). **d**, Representative traces from AM fibers recorded in skin-nerve preparation show increased firing following application of Hm1a (1μM) with quantification at right. Hm1a significantly increased firing during all forces tested, achieving statistical significance at 50 and 100mN (*** $p < 0.001$ with 2-way ANOVA, # $p < 0.05$ with Bonferonni post-hoc, n = 23, 23 and 18 fibers for vehicle and 13, 13 and 10 fibers for Hm1a at 15, 50 and 100 mN forces, respectively).

Author Manuscript Author Manuscript Author Manuscript Author Manuscript

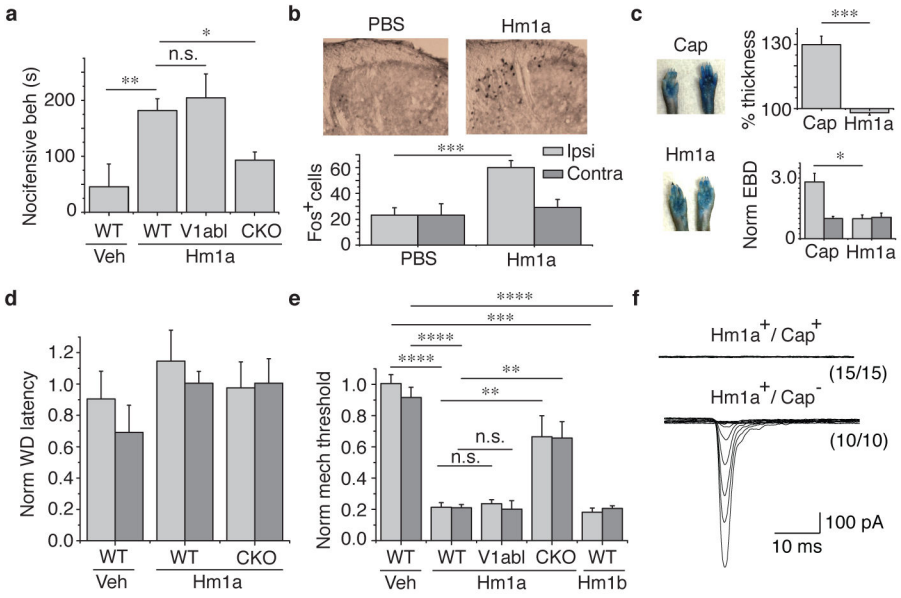

Figure 4. Hm1a elicits non-inflammatory pain and bilateral mechanical allodynia

a, Comparison of licking/biting behavior following intraplantar injection (10μl) of vehicle (PBS) (n = 6) versus Hm1a (5μM) (n = 10, $^{**}p < 0.01$). Behavior was unaffected by ablation of TRPV1 fibers (V1abl, n = 5) but significantly reduced in peripherin-Cre x Floxed-$Na_v1.1$ (CKO) mice ($^{*}p < 0.05$, n = 11). **b**, (Top) Representative histological sections and quantification of c-Fos immunoreactivity in spinal cord dorsal horn following intraplantar vehicle or Hm1a (5 μM) injection (n = 27 sections from 3 mice, $^{***}p < 0.001$). **c**, Capsaicin- or Hm1a-injected paws (right) next to uninjected contralateral controls (left). (Top right) Relative thickness of injected versus uninjected paws. (Bottom right) Evans blue dye (EBD) extravasation following capsaicin or Hm1a injection ($^{*}p < 0.05$). (d) Latency of paw withdrawal from noxious heat stimulus measured after intraplantar injection of vehicle or Hm1a (500nM). **e**, Mechanical response thresholds measured in paws ipsilateral (light grey) or contralateral (dark grey) to vehicle or toxin (500nM) injection (n = 5 for WT Veh, V1abl Hm1a and WT Hm1b; n = 7 for WT Hm1a; n = 9 for CKO Hm1a; $^{**}p < 0.01$, $^{***}p < 0.001$, $^{****}p < 0.0001$). **f**, Mechanically-evoked currents were observed from all adult mouse DRG neurons exhibiting sensitivity to Hm1a but not capsaicin (bottom), and not from those sensitive to both (top) (stimulus range from 1–9 micron displacement). Kinetic properties of mechanically-evoked currents in Hm1a responders were variable. Error bars represent mean ± SEM. P values based on unpaired two-tailed Student's t-test (panels b and c) or one-way ANOVA with post-hoc Tukey's test (panels a, d and e).

Author Manuscript Author Manuscript Author Manuscript Author Manuscript

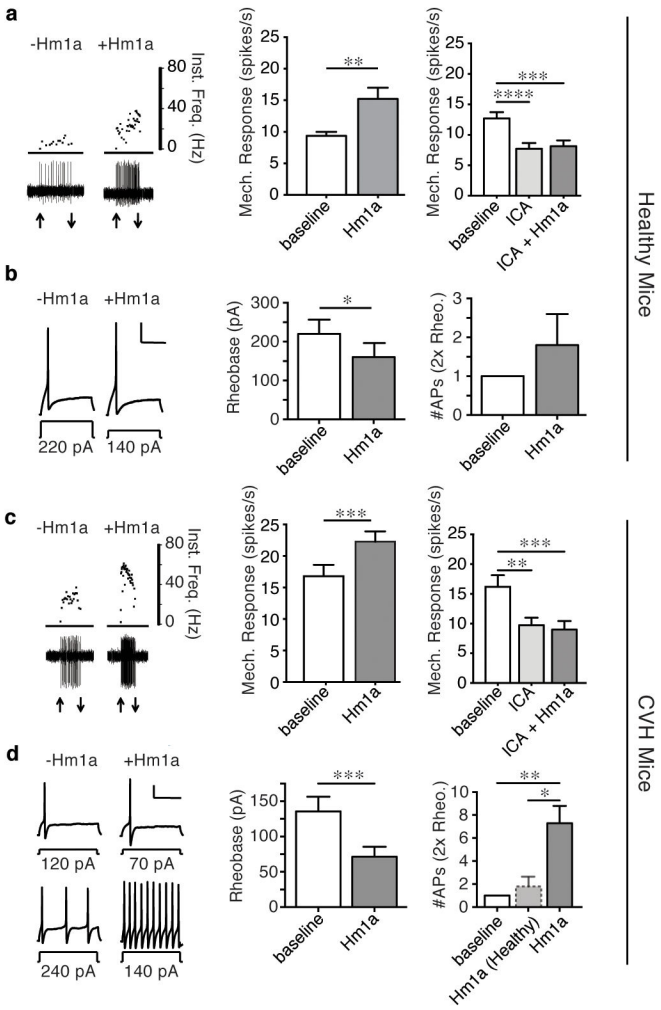

Figure 5. Colonic afferents display increased sensitivity to Hm1a in a model of IBS

a, (Left) Representative *ex vivo* single fiber recording from an Hm1a (100nM)-responsive high-threshold mechanoreceptive fiber from a healthy control mouse (arrows indicate application and removal of 2g Von Frey hair stimulus). (Middle) Group data from Hm1a-sensitive fibers (6/15, defined as ≥15% increase over baseline; $^{**}p < 0.01$; see Extended Data Fig. 5 for examples and group data from Hm1a-nonresponsive fibers. (Right) Group data from a population (5/10) of ICA-121432 (500nM)-sensitive afferents ($^{****}p < 0.0001$). **b,** (Left) Representative whole–cell current clamp recording of a retrogradely traced colonic DRG neuron in response to 500ms current injection at rheobase (the minimum current injection required to elicit action potential firing). Recordings were from the same neuron of a healthy control mouse before and after incubation with Hm1a (10nM). Scale bars = 250 ms, 20 mV. (Middle) Group data show significant reduction in rheobase following Hm1a application in a sub-population (5/11) of neurons ($^{*}p < 0.05$). Hm1a-responsive neuron defined as exhibiting ≥10% change in rheobase from baseline control. (Right) Hm1a increased the number of action potentials observed at 2x rheobase in these neurons, but not to a level that reached statistical significance. **c,** (Left) Responses from high-threshold colonic fibers from CVH mice before and after application of Hm1a (100nM). (Middle)

Author Manuscript Author Manuscript Author Manuscript Author Manuscript

Group data from Hm1a-responsive fibers (4/11, ***$p < 0.001$). (Right) Group data from ICA-121432-sensitive fibers (7/10, **$p < 0.01$). **d,** (Left) Representative Hm1a-responsive colonic DRG neuron in whole-cell current clamp. Addition of Hm1a reduced rheobase (top traces) and increased action potential firing at 2x rheobase (bottom traces). (Middle and right) Group data from Hm1a-responsive CVH neurons (7/11) showing toxin-mediated decrease in rheobase (middle, ***$p < 0.001$) or increase in action potential firing at 2x rheobase (right, *$p < 0.05$, **$p < 0.01$).